POLITECNICO DI TORINO

Master's Degree in Nanotechnologies for ICTs

Master's Degree Thesis

Bifacial/Tandem integrated energy harvesting and storage module

Supervisors

Prof. Andrea LAMBERTI

Candidate

Giulia GIANOLA

October, 2021

Summary

This master's thesis project is based on the realization of an energy harvesting and storage device able to produce and accumulate energy in a sustainable and green way. More in particular, the device is composed by a bifacial/tandem dye-sensitized solar module (for the harvesting) and by a supercapacitor (for the storage). These two electrochemical cells share a common electrode, through which the integration becomes possible.

The concept of bifacial and tandem properties for dye sensitized solar cells has been already exploited in literature during the last years. The idea proposed in this master's thesis activity is to combine both effects in order to obtain a bifacial and tandem integrated energy harvesting and storage module.

The main idea is therefore to achieve DSSCs characterized by high efficiency values, obtained by exploiting the combination between bifaciality and tandem properties. The goal is to get a new tandem-bifacial configuration, composed by a multilayer of vertically stacked cells. Here two adjacent DSSCs share the counter electrode, leading to the incoming radiation which is not absorbed by the first cell, to be collected by the following one. This causes an increase of the overall efficiency and a reduction of the losses since more radiation can be adsorbed. In order to have a multilayer structure like this, the need of transparency became crucial together with the requirement to have a counter electrode transparent and conductive on both sides.

Actually, the improved efficiency is not the only advantage. Also the concept of bifaciality has been enhanced. By using transparent materials, both photoanodes of the multilayer device can be front-illuminated by the incoming radiation, leading to a bifaciality index almost equal to one.

Moreover, the fabrication of a series connected module is achieved. This connection does not improve the cell's operation in terms of efficiency or photo-generated current. Actually, the upgrade concerns the open circuit voltage. Higher output voltages can be obtained, allowing the power supply for external devices (like sensors for instance) that usually need voltages greater than 2V to work.

Finally, the integration with a supercapacitor is carried on, so to allow the energy storage. A SC has been chosen as the accumulation part for the device because

of its advantages with respect to other kind of capacitors. Higher power density, durability, safety and reduced costs, make SC the best choice for this kind of devices.

At the same time, another point of interest concerns the choice of the materials used for the fabrication of the dye sensitized solar cell itself.

The main characteristics of DSSCs, which distinguishes them from other previous generations of photovoltaic cells, is based on the fact that they are self-sustainable power source with an immense capacity able to satisfy the energy demands of most indoor electronics. To this aim, dye sensitized solar cells have been developed as a kind of ambient photovoltaic cells capable of powering autonomous Internet of Things (IoT) devices.

According to this, Michaels et al. have recently studied and fabricated a DSSC based on materials different with respect to the standard ones, which turned out to be very powerful for indoor applications.

The highest values of efficiency are usually reached with a standard DSSC fabricated with a N719 dye and a iodine based electrolyte. Here, we propose the new couple exploited by Michaels and co-workers: a co-sensitized XY1:L1 dye and a copper based electrolyte. According to literature, higher efficiencies values have been achieved. Moreover, these materials allow to reach better performances in terms of indoor illumination, providing the suitable amount of power needed for IoT devices, which is typically low and therefore can be supplied under room light conditions.

In conclusion, an innovative and complete harvesting and storage device is here proposed. Particular attentions have been spent on the choice of anodes, counter electrodes, sensitizers and electrolytes in order to exploit an appropriate power supply cell for IoT systems.

Acknowledgements

To my parents, Daniela and Paolo, who let this experience possible. Thank you for your love, support and patience. Thank you for believing in me and for the help that you gave me from the beginning to now.

To my little sister, Sara. Thank you for being such a confident and a friend to me. I am so proud of the woman you became and so glad to share my life with a sibling like you.

To my best friends, Giulia, Yasmine and Maria Luisa. Without you, I would have turned out different. You are my strength and my happiness, thank you for all the experiences that we lived and we will live together.

To my friends and colleagues, Matteo and Simone. It has been a pleasure to share this adventure with you. Thank you for the motivation you gave me and for the help that I have always received.

To Roberto and all the other PhD students, who guided me all the way to reach my graduation. Thank you for sharing with me your knowledge, your experience and your time. This last six months have been hard, but they would have been surely harder without you.

To all my friends, to my boys and girls. I am so lucky to have people like you in my life. Thank you for our group study, for our holidays spent together, for each happy moments that we live and for the other that we will discover day by day.

Table of Contents

List of Tables

List of Figures

Chapter 1

Introduction

1.1 The demand for self-powered electronics

In the last decades, many steps forward have been made by the scientific community from a technological point of view. This progress is expected to be improved even more since the demand for electronic devices is increasing further and further. The quick transition of certain countries from undeveloped to developed makes the need for energetic furniture very important from an industrial point of view.

A part from the primary need for energy that allows to live in a comfortable way in the XXI century, also all those technologies clustered under the term "smart" are acquiring an increasing relevance year by year. Smart cities and the development of smart objects are nowadays of great importance, representing a kind of evolution for Internet's utilization. Let us imagine to live in a world where objects are in some way equipped with intelligence, enabling them to facilitate the manner in which we live our lives. We are talking about the already further investigated concept of Internet of things.

The IoT is becoming one of the major research and industrial subjects in the Information and Communications Technology (ICT) arena. According to the 9th International Conference on Next Generation Mobile Applications, Services and Technologies, the Internet of Things topic can be addressed to a “group of infrastructures interconnecting connected objects and allowing their management, data mining and the access to the data they generate” [1].

IoT devices are linked one with respect to the other through communication networks and it is expected that a huge amount of interconnected wireless sensors, actuators, personal data storage devices and household products will be installed in the next few years.

The peculiarity of this kind of smart objects lies in the fact that they need a low power to work. Therefore, common batteries or wired power source are not the

best choice for this kind of application. Moreover, another problem arises when we focus on the charging of this kind of devices. It is unthinkable to charge IoT devices daily or to replace batteries in microscale system like these, therefore new alternatives have to be found in order to harvest energy in a way suitable with the Internet of Things world.
Many researches have been carried on in order to find the best choice to power IoT systems. Studies have been performed on thermoelectric generators, mechanical energy harvesters and photovoltaic technology. The first category refers to those devices which take advantage of a temperature difference in order to convert the heat flux in electrical energy, exploiting the Seebeck phenomenon. However, thermoelectric generators are quite expensive, low efficient and could present very high output resistance. On the other hand, mechanical energy harvesters exploit the mechanical energy usually obtained by electromagnetic, piezoelectric and triboelectric generators. If compared to traditional electromagnetic generator they turn out to be cheaper, more flexible and simpler to fabricate. Nevertheless, view that IoT devices usually work in indoor conditions, it has been demonstrated that light could be the best solution to photogenerate electricity and power a load. Photovoltaic technologies convert the incoming radiation in electrical energy, through the presence of a sensitizer which exploits the absorption of light to generate electrons.

1.2 The PV technology

For many years, fossil fuels were the worldwide most employed energy source. However, the environmental issue has to be taken into account and some alternatives have to be found. The increasing level of pollution and the more and more alarming situation around the global warming topic impose new ways to provide energy, in order to overcome the problem and move towards a low-carbon society.
To this aim, the Photovoltaic industry is playing a relevant role. Up to now, we split the PV framework in three different categories, called generations. The first one is related to crystalline silicon technology and it is nowadays the most exploited solution, since the electric energy production is very appealing if compared to the one of fossil fuels. The second generation concerns the thin films technology, based on amorphous Silicon, Cadmium Telluride (CdTe), copper indium diselenide (CIS) and copper indium gallium diselenide (CIGS). The third and last generation is based instead on dye sensitized solar cells (DSSCs), organic solar cells, Perovskite solar cells, quantum dot solar cells and copper zinc tin sulphide (CZTS) solar cells. In figure 1.1 all the relevant PV technologies are shown, in terms of their efficiencies, according to National Renewable Energy Laboratory [2].
In particular, among all the PV technologies, dye sensitized solar cells demonstrate

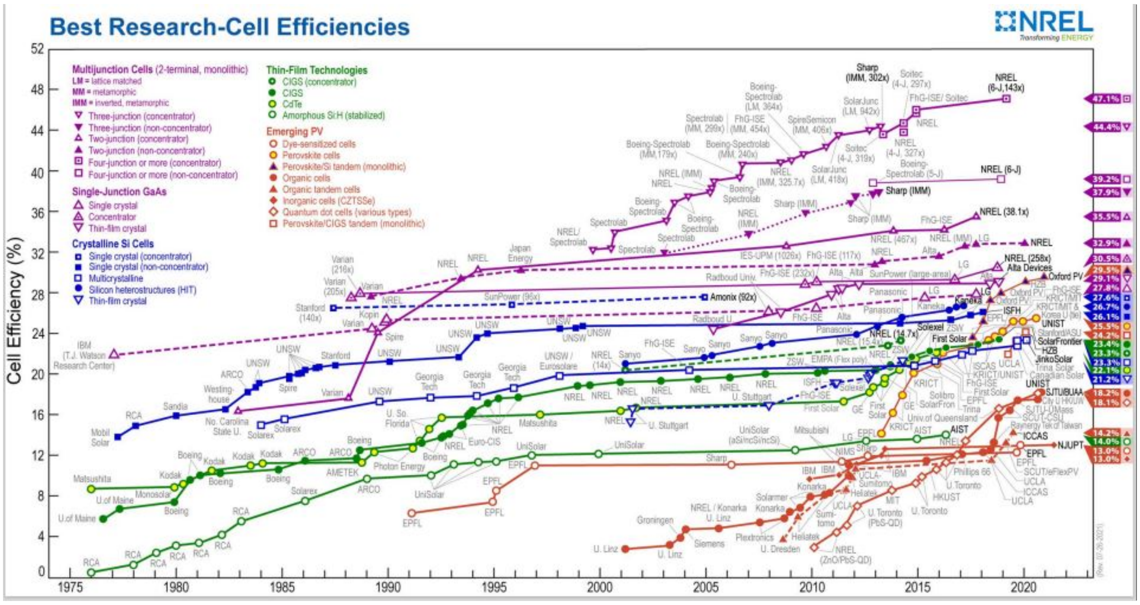

Figure 1.1: NREL (National Renewable Energy Laboratory) Chart of power conversion efficiencies of best research solar cells from 1975 to the present for various photovoltaic technologies [2]

good efficiency values and low fabrication costs.

The issues which is always hidden in PV technologies concerns the fact that they require solar light to work. This limit the time window of utilization, view that the illumination condition depends on weather, incidence angles and day/night duration. However, recent studies have demonstrated that DSSCs show excellent performance under indoor environment with an artificial light source compared to other solar cell technologies. This can be an advantage especially if we consider the operating condition required for smart objects. IoT devices usually require a quite low power to work, therefore it can be supplied by a DSSC illuminated with ambient light, since the cell turns the room light directly into electricity without external power supply.

Let us focus in particular on the top right side of figure 1.1, actually where multi-junctions solar cells lie. MJSC are based on vertical stacked pn junctions, each one made by different semiconductor materials. The use of different materials allows the absorbance of a broader range of wavelength, since each material is characterized by its own bandgap. In this way, each single cell will be sensitive to a certain range of photon's wavelengths, allowing the reduction of losses since the radiation that it is not absorbed by the first pn junction could be eventually absorbed by the underlying solar cells. An example can be observed in figure 1.2.

The kind of structure of the MJSC explained so far can be addressed to the category

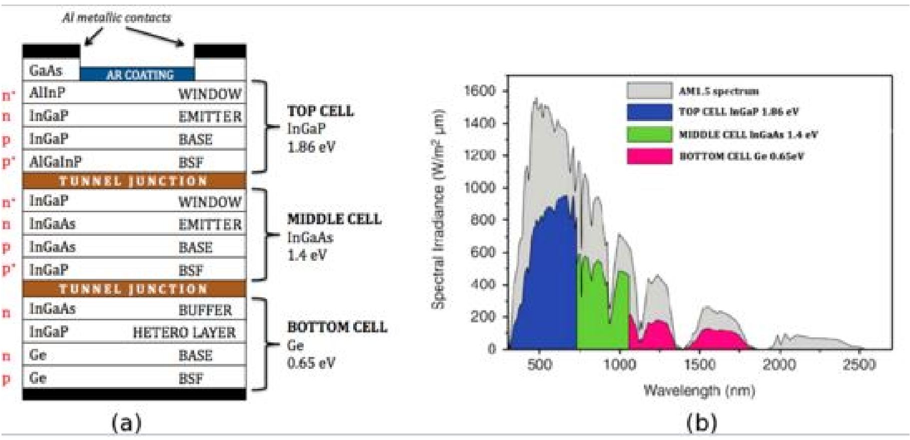

Figure 1.2: a) The structure of a multi-junction solar cell. b)Graph of spectral irradiance E vs. wavelength λ over the AM1.5 solar spectrum, together with the maximum electricity conversion efficiency for every junction as a function of the wavelength [3]

of "tandem solar cell", according to literature. In particular, we call tandem those cells in which at least two stacks of absorber are present, in such a way to improve the collection of incoming light. In particular, if we have a structure where two pn junctions are present, one with high bandgap material and the other with a low one, the irradiation have to hit at first the absorber with high bandgap in order to absorb high energy photons. Then the first absorber should be transparent in such a way that low energy photons (photons with energy lower than the bandgap of the first material) can be collected by the underlying low-bandgap layer.
In practice, this kind of cells exploit the rule of thumb hidden behind the photon absorption phenomenon. Photons with an energy lower than the material's bandgap do not undergo collection at all. On the other hand, photons with an energy higher than the bandgap of the absorber layer can generate electrons, since photons have enough energy to overcome the bandgap of the material. The mechanism of absorption leads in fact to the excitation of one electron to a state above the bandgap, but usually this extra energy is lost because of a phenomenon called relaxation. Here, collisions occur and loss of energy happens. However, in multi-junction solar cells, different materials are employed and therefore light can be harvested at different wavelengths according to the materials' bandgap. Multiple photon capture processes occur, converting some of the energy lost during relaxation in useful energy.

In fact, as we can see from figure 1.3, the incoming spectrum is split between the cells, in such a way that each solar cell is optimized to each section of the spectrum.

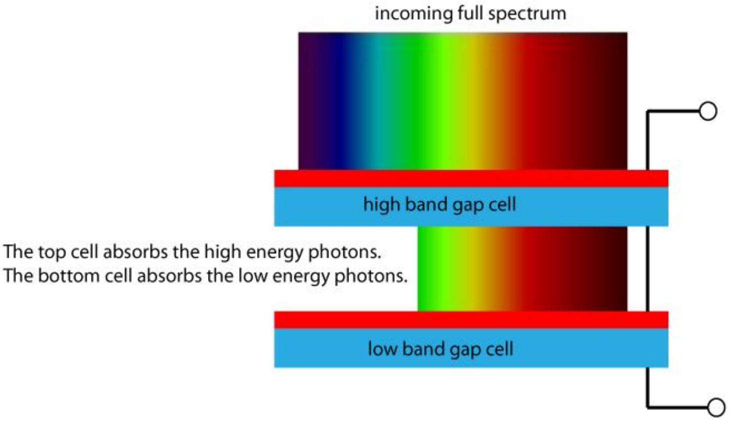

Figure 1.3: Series connected tandem solar cell [4]

Therefore, adding more devices allows for each device to be optimized to a narrower spectrum giving a higher overall efficiency.

1.3 Improving the DSSC

According to literature, the standard architecture of a dye-sensitized solar cell presents a cell composed by a photoanode where a layer of nanostructured TiO_2 paste is deposited. Then the titania oxide is covered with a sensitizer, namely an organic dye, which enables the photon to electron conversion. On the other side the cathode is usually powered with a catalyst layer and the whole cell is sandwiched in such a way to be filled with an electrolyte, promoter of the redox reactions which occur inside the electrochemical cell. However, we will better analyse the architecture and the working mechanism of a single dye-sensitized solar cell in section 2.

The focus point of this section is in fact related to the possible improvements to which a DSSC can be subjected.

A possible strategy, largely studied in the last years by the scientific community, concerns the concept of bifacial solar cell [fig. 1.4].

The main idea behind this PV technology consists in the possibility to both front and rear illuminate a dye-sensitized solar cell in such a way to harvest energy independently on the irradiation provenience. To this aim, the cell is structured in such a way to have a FTO covered glass that behaves as anode after the deposition of a Titania paste. Then the sensitizing dye is put over the TiO_2 layer in order to make the anode photoactive. Finally, the cell ends with a counter electrode, which has to be rigorously transparent so that the illumination can reach the

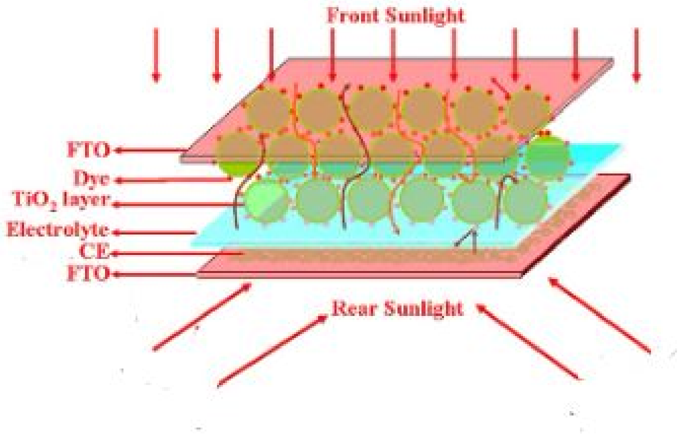

Figure 1.4: Architecture of a bifacial DSSC [5]

photoanode even if it comes from the rear side. In fact, what we observe in figure 1.4 is a standard DSSC that could behaves as a bifacial one if its components are transparent. For instance, by substituting the commonly used Platinum counter electrode and the electrolyte with something transparent it is possible to illuminate the device on both sides.
This kind of cells can be used for instance as windows, where one side is exposed to the outdoor natural light while the other one absorbs the artificial light coming from inside. In such a way the performances improve without changing to much the design.

1.4 Aim of the thesis activity

According to what said before, the focus of this thesis activity is therefore to fabricate and characterize a device able to power another device, such as a smart object. As already mentioned, the choice lies with PV technology, DSSC more precisely.
At this point, what we are really interested in is to produce a new dye-sensitized solar cell which improve its photon-to-electron conversion behaviour.
The idea bases on the combination of tandem solar cells and bifacial dye-sensitized solar cells, which working mechanisms and architectures were already explained in the previous sections. In particular, we want to present an innovative design for a DSSC in which two cells are vertically stacked one on top of the other [fig, 1.5].
The key element of its construction is based on the sharing of the counter electrode

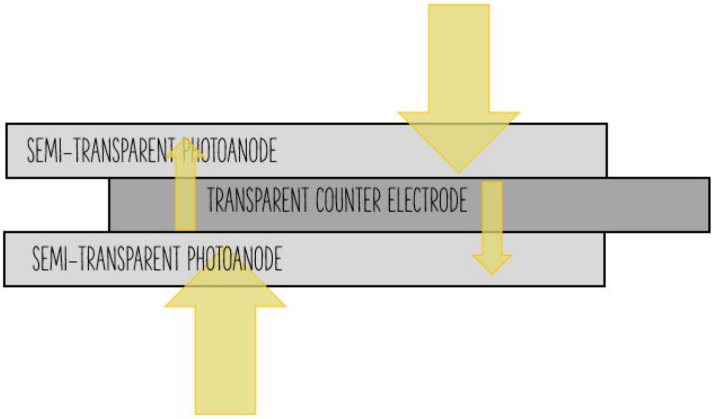

Figure 1.5: Architecture of the new tandem/bifacial DSSC

between the top cell and the bottom one. But not only the CE has to be shared between them, it has to be transparent too in such a way that the radiation which is not absorbed by the first cell can be harvested by the second one.

Moreover, view that we want to enforce in this new cell also the bifaciality idea, the photoanodes are made transparent. In this way, not only the absorption losses are reduced because of the tandem configuration, but also a bifacial cell is obtained. Both front and rear illumination allows the activation of the photon-to-electron conversion mechanism and, because of the symmetric structure of the cell, a bifaciality index almost equal to one could be achieved (more details in section 2.5).

The combination of bifacial and tandem properties allows therefore to increase the efficiency, but this is not the only goal that we want to reach. During the course of this thesis project, we will try to develop a series connected module in order to obtain a higher output voltage with respect to the one of a single cell. Such a series allows for bigger open circuit voltage values, required for the powering of an external device that we want to sustain with the PV technology.

Together with these studies concerning the architecture of the solar cell, also another kind of analysis concerning the choice of materials will be performed.

According to literature [6] optimized solar cells can be obtained by exploiting a new dye-electrolyte couple. In particular, using a copper based electrolyte and a co-sensitization of XY1 and L1 dyes, higher efficiencies, but especially higher output voltages, under indoor illumination can be obtained. More details will be given in section 2.6.

Until now, we have focused our attention to the energy harvesting mechanism, but actually we are also interested in the storage part.

Today's world is full of wireless devices and sensors that use perishable batteries

which are dangerous for the environment and very costly to change. Solar technologies take action to find a solution to this problem by producing dye-based photovoltaic cells (DSSC) to power wireless electronics instead of standard PV technologies that are not well-matched to wireless applications.
It has to be taken into account that together with the energy harvesting, also its storage plays a crucial role. Once, batteries were the most used electrochemical energy storage system. However, this kind of accumulation devices present many drawbacks such that the scientific community is on its way to replace batteries with a new type of EES system: the supercapacitor.
A supercapacitor combines both batteries and capacitors effects into a single device, providing advances in the energy storage system. In particular, looking at figure 1.6 it is possible to better appreciate where supercapacitors locate if compared with standard capacitors or batteries.

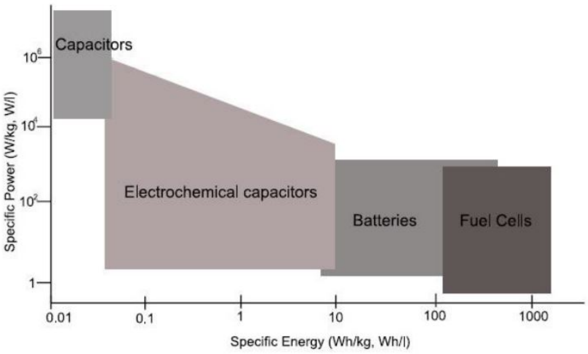

Figure 1.6: Ragone plot for different energy storage devices [7]

From the above Ragone plot we can observe that SC exploits better power densities than batteries, but lower energy densities. However, they offer many other advantages over standard batteries: improved durability, enhanced safety and reduced costs (further details will be presented in section 3).
At this point, what we want to obtain is an integrated energy harvesting and storage device composed by a tandem/bifacial series connected module and a supercapacitor. In this way, we will obtain a unique device able to produce, store and deliver energy.

Chapter 2

Dye Sensitized Solar Cell

Dye-sensitized solar cells, also called Gratzel cells in memory of its inventor, belong to the category of low-cost solar cells which are able to generate electricity at an oxide electrode if an organic dye is illuminated.
The first official reference of DSSC appeared in a US patent in 1977, but the true turning point was given by the professor Micheal Gratzel during the 1980s thanks to his work on metal oxide sensitization until reaching the first efficient dye-sensitized solar cell in 1991, which was based on a nanometric titanium dioxide (TiO_2) layer and on a polypyridyl complex of ruthenium used as the light absorber.
From that moment on, in the last two decades, the field concerning DSSC is growing faster and faster, becoming one of the main argument touched in the scientific community. It suffices to think that nowadays, two or three research articles about this topic are published every day. In figures 2.1 and 2.2, a simple and limited literature search illustrates the growth of the number of research papers and patents over the last years [8].

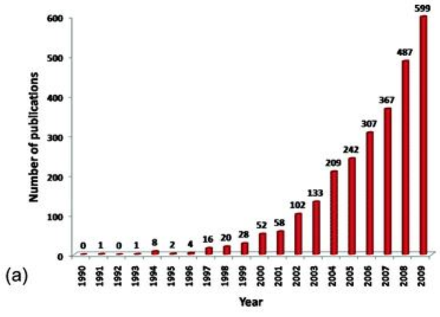

Figure 2.1: Number of DSSC research articles

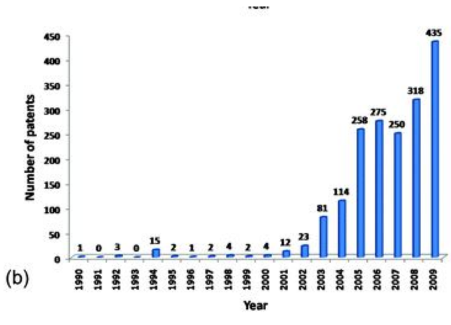

Figure 2.2: Number of DSSC patent families

The principle of DSSC has also become a part of the core chemistry and energy science teaching. Text books have sections or chapters dealing with DSSC and laboratory kits have been developed for educational purposes. Not only energy science but also photochemistry, photoelectrochemistry, materials science, and transition metal coordination chemistry have significantly benefitted from DSSC research.

With time, however, the chemical complexity of the DSSC device has become more and more evident.

The DSSC is a good example of a molecular system where the function of the overall device is better than predicted from the sum of the properties of its components. There are complex interactions between the device components, in particular, at the oxide/dye/electrolyte interface, but the interactions also depend on external variables such as solar irradiation, temperature, and device working conditions. Also inherent in the devices are multiscaling properties, both in time and in length, which need to be characterized and handled for the optimization of the overall device performance.

As said before, dye-sensitized solar cells are becoming more and more relevant in the everyday life, also because they are able to expand the range of applications where conventional solar cells are unsuitable.

In a world dominated by traditional silicon based and by inorganic thin film technologies, DSSCs can compete with several advantages. View their stable performances, DSSCs are a good choice in nonstandard conditions of temperature, irradiation, and solar incident angle; they are affordable in economical terms for low-cost manufacturing processes and in terms of quantity and availability of raw materials. Moreover, dye-senstized solar cells are very attractive in terms of esthetic possibilities for architectural elements and building integration. In fact, DSSCs could represent solutions for the integration of photovoltaics in places where landscape restrictions have so far limited their application or for fashion reasons. The manageability of these cells could fit the standards even for the integration in the automobile and nautical sectors and additionally give major input to the intelligent sensors industry.

The beneficial aspects that can be exploited by using this kind of cells are resumed in the following [9].

- Low-light performance → A wide array of lighting conditions is possible making DSSCs suitable for shaded and diffuse light locations, without suffering from angular dependence of sunlight or light;

- Optimised performance → Materials and dyes can be tuned for optimisation in a variety of both indoor and outdoor lighting conditions;

- Higher temperature performance → Efficiency does not degrade with increased temperature, meaning the possibility to continuously and efficiently harvest energy in direct sunlight;

- Low energy manufacturing process → Cells are manufactured using a low-energy consumption and high-efficiency manufacturing technique;
- Ecologically friendly solar → Cells use inexpensive and eco-friendly nano-materials without concern about shortage of resources;
- Variety of substrates → Cells are produced on a thin film, flexible, robust, plastic substrate. DSSC can also be applied to metal and glass substrates
- Versatile product integration → Cell indoor modules are highly flexible, durable and lightweight; as a result they are very versatile and can be incorporated into a wide variety of products;

2.1 Architecture and working mechanism of DSSCs

The structure of a dye-sensitized solar cell can be explained according to what illustrated in figure 2.3 [10]:

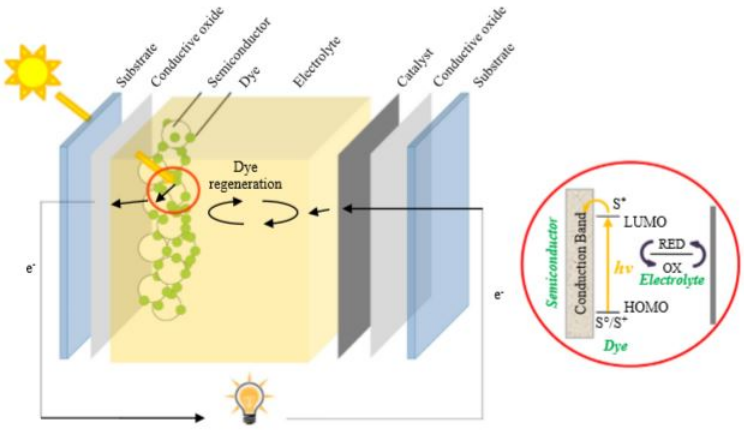

Figure 2.3: Sketch of the DSSC structure and operational mechanism

It is important to focus on the fact that in a dye-sensitized solar cell each component has a special task and as a consequence the choice of the used materials is very crucial:

- Electrodes: the anode consists of a glass plate which is coated with a transparent conductive oxide (TCO) film, like indium tin oxide (ITO) or fluorine tin oxide (FTO), and which has the role of charge collection and electrical connection. It essentially bears a continuous network of sintered titanium dioxide nanoparticles, such that this porous network offers an inner surface that is a thousand times greater than the equivalent flat area, and acts like a “light sponge” in which sunlight can get trapped;

- Catalyst: a layer (in most cases it is platinum) deposited, usually through the sputtering physical vapor deposition technique, on the cathode in order to enable the redox reaction. Since a very small quantity of catalyst is needed, the electrode could remain transparent because of the very thin deposited layer;

- Electrolyte: it is composed by a redox mediator and a solvent in order to induce dye regeneration. The most common choice for redox mediator is the combination iodide/triiodide, but view its low redox potential and its high corrosivity also Cobalt and Copper could be used, while the solvent is typically a nitrile one;

- Dye: it is a photosensitizer made of N719, Di-tetrabutylammonium cis-bis(isothiocyanato)bis(2,2'-bipyridyl-4,4'-dicarboxylato)ruthenium(II), which is the ammonium salt of N3 dye. Dye molecules are anchored onto the high surface area semiconductor in order to absorb electromagnetic radiation coming from the light source.
- Metal oxide: thin layer of TiO_2 nanoporous anatase which exhibits a high surface area because of its high porosity in order to guarantee the charge transport from the dye to the electrode.

In order to explain the working mechanism hidden behind a dye-sensitized solar cell, let us taking into account what happens from an energetic point of view inside the cell, focusing on all the energy levels which are involved during the photoelectron generation. The light coming from both natural and artificial sources, is captured by a photosensitizer that is adsorbed on a thin-layer of a nanocrystalline semiconductor (usually TiO2) placed on the anode. Upon excitation, the photosensitizer transfers an electron to the semiconductor and from there to a back contact; the oxidized dye is subsequently reduced by means of a suitable redox couple, which is in turn reduced at the cathode; finally, a connection between the two electrodes gives rise to an electric current.
Figure 2.4 shows in more detail how effectively a dye-sensitized solar cell works [11]:

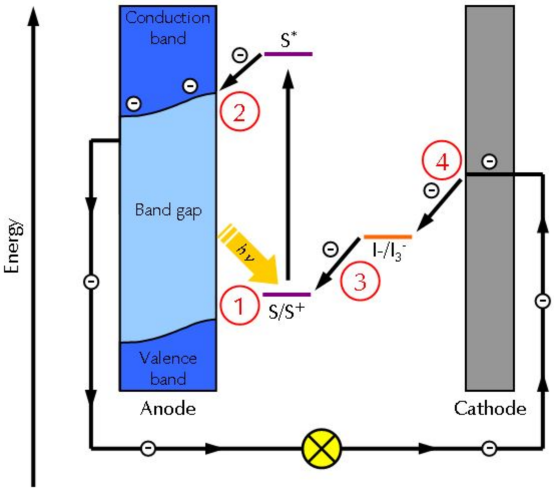

Figure 2.4: Energy diagram of a dye solar cell

The dye molecule is initially in its ground state (S). Thanks to incoming light, dye molecules get excited from their ground state to a higher energy state (S*):

$$S \rightarrow S^* \tag{2.1}$$

Now the excited dye molecule is oxidized and an electron is injected into the conduction band of the semiconductor:

$$S^* \rightarrow S^+ + e^- \tag{2.2}$$

Then, the oxidized dye molecule is again regenerated by electron donation from the iodide in the electrolyte:

$$S^+ + \frac{3}{2}I^- \rightarrow S + \frac{1}{2}I_3^- \tag{2.3}$$

In return, iodide is regenerated by reduction of triiodide on the cathode:

$$\frac{1}{2}I_3^- + e^- \rightarrow \frac{3}{2}I^- \tag{2.4}$$

Moreover, DSSCs produce more power when the temperature increases and can harvest light beams coming from all angles, which allows them to work even in the presence of diffuse light.

2.2 Characterization techniques and parameters

As for all other cells belonging to the PV family, the most exploited way to characterize a DSSC is through a potentiodynamic measurement, namely current-voltage (IV) measurement. This kind of technique allows to measure the photo-generated current harvested inside the electrochemical cell by adopting a Keithley SourceMeter. To this aim, a steady state measurement in DC is performed, where thanks to small increments of the applied potential the output current can be measured. Usually, a precise region is examined exploiting a specific potential window: from a slightly negative potential to a positive one, larger with respect to the open circuit condition.

Moreover, the measurements can be performed both in dark and under illumination conditions, but in order to achieve the photo current generated inside the cell the illumination is required. To this aim, a sun simulator is used and the solar cell or module is put under the light source such that the active part of the PV cell could absorb light and generate current.

In this regard, let us at first list the standard test conditions that are usually employed for testing PV solar cells:

- 100 $mWcm^{-2}$ radiation intensity;
- 25 $°C$ PV device temperature;

- Air mass 1.5 (AM1.5)[1]

In these conditions, the cell connected to the Keithley multimeter allows to obtain an IV curve with the following shape [fig.2.5].

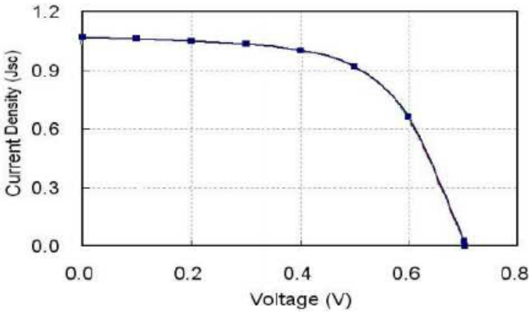

Figure 2.5: IV characteristics of a DSSC [12]

Actually, there are some kind of non ideality effects that can be observed when performing an IV measurement. In fact, the solar cell may also contain series and parallel (or shunt) resistances which modifY the output characteristics. For ideal solar cell, $R_s = 0\ \Omega$ and $R_{sh} = \infty$, but in reality, we have losses due to material resistance while current goes between two electrical contacts (R_s). We also have defects and trapping centers (electron and hole trapping) particularly at interfaces which decrease the collected charges (R_{sh}). View that, in a circuit, a resistor is responsible for losses of energy, then series and shunt resistances are parasitic elements which causes losses in the solar cell. Both series and shunt losses degrades the fill factor and efficiency of a solar cell as we can observe in figure 2.6.

In particular, the fill factor (FF) is the quantity that defines the quality of a solar cell. In practice, it compares the maximum power to the theoretical power that could be get at both short circuit current and open circuit voltage conditions [eq. 2.5], as we can see in figure 2.7.

$$FF = \frac{P_{max}}{V_{OC} J_{SC}} \tag{2.5}$$

Where V_{OC} [V] is the open circuit voltage, J_{SC} [mA/cm^2] is the short-circuit current density.

---

[1] The air mass coefficient defines the direct optical path length through the Earth's atmosphere, expressed as a ratio relative to the path length vertically upwards, i.e. at the zenith. The air mass coefficient can be used to help characterize the solar spectrum after solar radiation has traveled through the atmosphere.

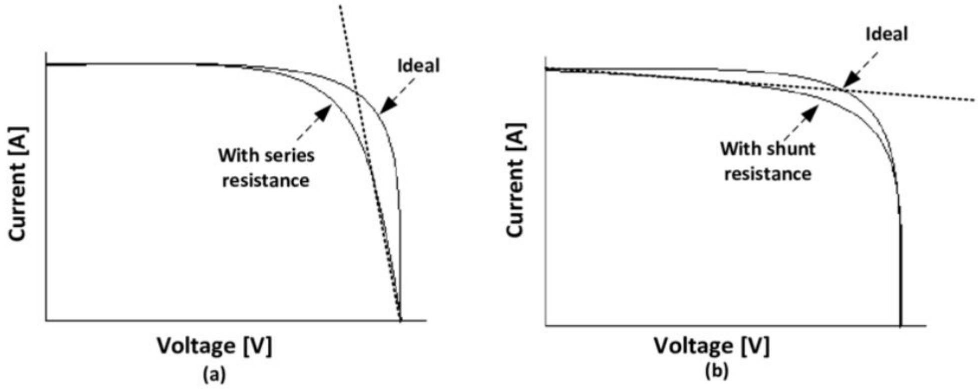

Figure 2.6: The effects of series (a) and parallel (b) resistances on the IV characteristic [13]

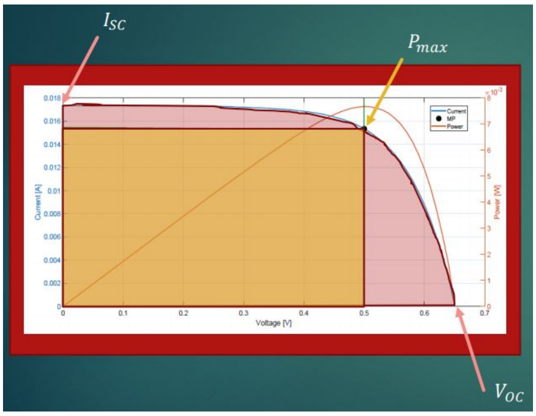

Figure 2.7: Graphical representation of the fill factor: $FF = \frac{yellow\ \ area}{red\ \ area}$

From each of these parameters, and knowing the incident power P_{in} $[mW/cm^2]$ of the illumination source, the efficiency η of the DSSCs can be obtained using eq. 2.6.

$$\eta = \frac{FFV_{OC}J_{SC}}{P_{in}} \tag{2.6}$$

The efficiency, expressed as a percentage, is one of the most important parameters and it practically defines the total amount of electrical power harvested for a given quantity of solar power directed towards the active part of the cell.

As introduced before, all these parameters can be obtained with an IV measurement, but it is not the only technique that we can exploit. In the following, elEctrochemical impedance spectroscopy analysis will be performed too.

EIS is an electrochemical measurement for the impedance of a device in dependence of the AC potentials frequency. More in particular, an AC voltage is applied to the system and the AC current output is analysed in terms of the frequency. Therefore, thanks to the presence of a frequency response analyser (FRA) together with the potentiostat measurement, the impedance of the system can be computed through the ratio between the AC voltage and the AC current. View that both $V(\omega, t)$ and $I(\omega, t)$ can be expressed in terms of complex numbers, then the overall impedance can be calculated as:

$$Z(\omega, t) = \frac{V(\omega, t)}{I(\omega, t)} = \frac{V_0}{I_0} e^{j\theta} = |Z(\omega)| e^{j\theta} = Z'(\omega) + jZ''(\omega) \tag{2.7}$$

where $Z'(\omega)$ and $Z''(\omega)$ are respectively the real and the imaginary part of the system's impedance. These two EIS data are used to build the Nyquist plot, where Z" is reported as a function of Z' in the complex plane [fig. 2.8].

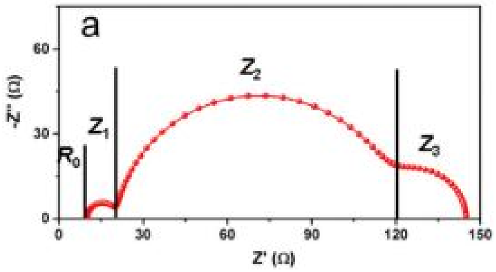

Figure 2.8: Example of Nyquist plot [14]

By looking at the above figure we can observe different semicircles representing the different impedance contributions coming from the electrochemical system. In fact, the biggest advantage of EIS analysis is that it allows to separate the influences of different components, namely the contribution of electron transfer resistance, double layer capacitance, diffusion impedance of the redox species into the electrolyte and so on. All these components can be visually observed by representing the equivalent electrical circuit of dye-sensitized solar cell [fig. 2.9].
The meaning of each single contribution is reported here in the following:

- R_{STCO} [Ω] ohmic series resistance of the cell;
- C_{CO} [F]substrate contact capacitance at the interface between the TCO and the TiO_2 film;
- R_{CO} [Ω] substrate contact resistance at the interface between the TCO and the TiO_2 film;

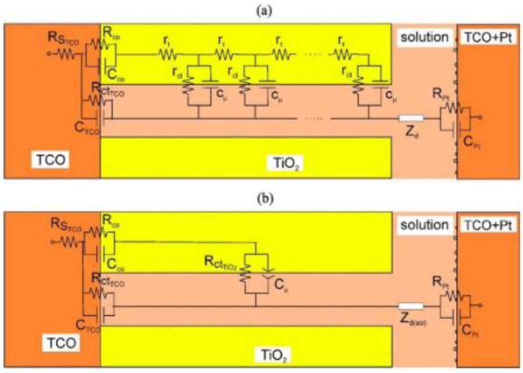

Figure 2.9: Equivalent electric circuit based on the transmission line model for a DSC. (b) Simplified equivalent circuit valid when TiO_2 is in high conductance state. [14]

- R_{ctTCO} [Ω] substrate charge transfer resistance;
- C_{TCO} [F] substrate double layer capacitance at the TCO/electrolyte interface;
- R_{ctTiO_2} [Ω/m] recombination charge transfer resistance at the TiO_2/electrolyte interface;
- c_μ [F/m] photoanode chemical capacitance, that stands for the change of electron density as a function of the Fermi level;
- Z_d [Ω] electrolyte diffusion impedance, accounting for mass transport of redox species in the electrolyte;
- R_{Pt} [Ω] counter electrode charge transfer resistance;
- C_{Pt} [F] counter electrode charge transfer capacitance.

In conclusion, EIS will be used in the following sections of this thesis, in order to evaluate the relevant impedance of interest of the electrochemical cells that will be analysed.

2.3 Experimental section

At this point, we can focus on the fabrication method used for a dye-sensitized solar cell.
There are many ways to make a DSSC, with many combinations of materials and designs. For instance, some people may make cells open to the air, while others may choose to deposit the titania on their own. Some may prefer natural dyes

instead of ruthenium dyes, and carbon cathodes instead of platinum cathodes, to make inexpensive solar cells for school activities. [15]
In a laboratory context, the main aim is to produce a cell which has small volume, tuneable properties and repeatable recipes.

Front and back electrodes shaping:
As mentioned before, the typical substrate for making DSSCs is a glass plate coated on one side with a Transparent and Conductive Oxide (TCO) layer. However, the TCO layer is conductive only on one side, that can be found by scratching each side of the glass with a plastic spatula or even with the fingernail: the conductive side is the one that feels a little sticky. Once that the conductive side has been discovered, the electrode has to be cut with a glass knife or with a diamond cutting edge according to the desired size. In our case, the used glass electrode is provided by Solaronix and it labeled with the name TCO22-7. In particular, the transparent and conductive oxide is in this case FTO, namely a fluorine tin oxide. The number "22" specifies the thickness (in mm) of the electrode. On the other hand, "7" is the sheet resistance per ohm square, the resistance of the thin film which is almost uniform along the whole surface.

Front and back electrodes cleaning:
Once that both electrodes have been shaped, they have to be cleaned with specific glass detergents. The technique used for this kind of process is the following one and all the steps are performed with an ultrasonic deaner that works at 40 kHz. At first, the electrodes are dipped in a solution of water and soap for 30 minutes and then rinsed, in order to clean possible oily traces coming from the cutting step. Subsequently, the glass substrates are immersed in Acetone for 30 minutes and after rinsed. Finally, they are put in Ethanol for 30 minutes and then rinsed again. All these steps are required in order to be sure to eliminate any possible residual from the electrodes' surface. After all the cleanings, electrodes are dried with a nitrogen flux and then the glass layers are disposed on a hot plate for 10 minutes at $100°C$ in such a way that all the used solvents evaporate.

The TiO_2 semiconductive layer:
The second step concerns the formation of a TiO_2 anatase slurry made of TiO_2 anatase powder, organic solvent like ethanol, deionized water and a surfactant, such that nanoparticles stay separated and do not agglomerate. Here we use already prepared pastes given by Solaronix. According to the utilization, we may exploit both transparent and opaque TiO_2 pastes which characteristics are reported here below according to Solaronix data sheet [tab. 2.1].
Now the electrode has to be coated with the TiO_2 slurry prepared in the previous step. In particular, at first the electrode is masked with a tape $\sim 70 \div 80\ \mu m$ thick

Table 2.1: TiO_2 paste characteristics [16]

	Ti-Nanoxide D/SP	Ti-Nanoxide T/SP
Resulting layer	opaque	transparent
Anatase titania particles	15-20 nm	15-20 nm
Diffusing titania particles	>100 nm	none
Concentration	$\sim 18wt\%$	$\sim 18wt\%$
Solvent	ethanol	ethanol
Binder	organic	organic

in order to confine the active material. Then the paste is deposited by exploiting the Doctor-Blade technique: a portion of paste is applied near the top edge of the TCO glass; with a rigid squeegee the paste is spread across the plate. The gap between the strips of tape should be filled with a layer of titania paste. The operation is repeated until a reasonably homogeneous layer is obtained.
The adhesive tape used as mask is removed and the solvent evaporates by using an hot plate held at 100°C for some minute.
Now it is time to sinter the nanoparticles. This operation is made with a muffle oven held at 450°C for about one hour. While heating up, the titania layer turns brown/yellow and releases fumes. This corresponds to the evaporation and combustion of the non-toxic chemicals used in the paste formulation. Once the process is finished, the heating device has to be cooled down before removing the fired electrode in order to avoid the glass to break as a consequence of a sudden change in temperature.

Sensitization:
The front electrode is immersed in the dye solution in order for dye to anchor on NPs as a monolayer. In standard cases we will use a ruthenium based dye: di-tetrabutylammonium cis-bis (isothiocyanato) bis(2,2'-bipyridyl-4,4'-dicarboxylato) ruthenium(II), easily called N719 [fig. 2.10].
The dye can be prepared with 0.3 mM of N719 in Ethanol. In particular, using a 50 ml falcon and noticing that the molecular weight of N719 is 1188.6 g/mol, 17.83 mg of ruthenium dye are necessary. This amount is put in 50 ml of ethanol and then sonicated for 10 minutes.
At this point the photoanodes are immersed in the dye for $\sim$ 18 hours. The longer the electrode soaks in the dye, the better dyed the titania will be. After being removed from the dye solution, the electrode must be washed with ethanol and dried from the excess dye.

The counter electrode:

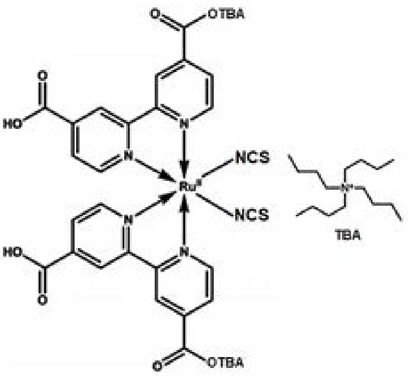

Figure 2.10: Chemical structure of N719 Dye. Chemical formula: $C_{58}H_{86}N_8O_8RuS_2$

In order to complete the assembly of the DSSC, a cathode is required; in particular, it is often referred as a counter electrode which needs to be drilled in order to create the hole through which inject the electrolyte. This procedure is performed by using an appropriate drill bit for glass with typical diameters from 1 to 5 mm, in order to produce one single hole through which the chamber of the electrochemical cell can be filled via vacuum filling.
Then, the counter electrode has to be coated with a Pt layer which gives the best performances. This step occurs because the cathode needs a catalyst for the dye regeneration. Platinum is deposited on the counter electrode surface thanks to sputtering deposition: the sample is placed in the reaction chamber where vacuum holds and a Argon-based atmosphere is present. The Pt target is bombarded by energetic partilces of a gas and a deposition of few nm is performed on the sample. In particular, a current of 30 mA is applied to let the target be bombarded and the thickness of the deposited layer can be regulated by controllingt the amount of time to which the substrate is subjected to sputtering. For opaque counter electrode, 80 s of sputtering are performed, while for transparent counter electrodes a deposition of 10 s is enough.

Cell assembly:
Two different procedures can be performed for the assembly of the cell. The "open-cell" method consists in pressing together two electrodes and the resulting stack is filled with the electrolyte by capillary effect. The second technique consists in sealing the two electrodes together and the electrolyte is injected via holes drilled through the cathode. Here the second technique is used and a gasket is required to limit the area of the chamber where the electrolyte will be injected. It can be obtained by a hot-melt film (Meltonix) with a shape corresponding to the active

area of the cell and sandwiched between the two electrodes. At this point the cell is sealed thanks to the application of an high heat and pressure, performed through an hot press or similar held at 110°C; in this way, after few seconds, the hot melt material glues the two electrodes together.

Electrolyte injection:
The gap between the two electrodes can now be filled with electrolyte. A pump is used and the electrolyte fills the cavity where vacuum has been created. Finally, a small glass cap will be used to seal each hole with another piece of sealing film. At this point the cell is completely fabricated and it can be tested.

2.4 Results and data analysis

Let us at first analyse the results obtained for a standard DSSC, fabricted exploiting the following characteristics:

- Opaque TiO_2 photoanode obtained with Ti-Nanoxide D/SP from Solaronix ;
- Dye N719;
- Active area of 1 cm^2;
- Electrolyte I^-/I_{3-};
- Pt counter electrode through sputtering 30mA/80s;
- Electrolyte injected through drilled hole and cell sealed with Meltonix.

In particular, we perform the analysis on five different photoanodes [fig. 2.11], in such a way to produce an estimate on characterization parameters. Moreover, we also evaluate the amount of both sintered titania and absorbed dye in such a way to have an averaged esteem of the active part of the cell [tab. 2.2].

Table 2.2: Average weights of the glass electrodes w/wo titania/dye

Electrode	FTO weight [g]	weight after TiO_2 [g]	weight after dye [g]
1st	2.76630	2.76785	2.76811
2nd	2.79422	2.79602	2.79617
3rd	2.77967	2.78060	2.78099
4th	2.78976	2.79205	2.79224
5th	2.77690	2.77835	2.77878
Average	2.78137	2.78294	2.78326

From the above table we can extract some relevant information. The average weight

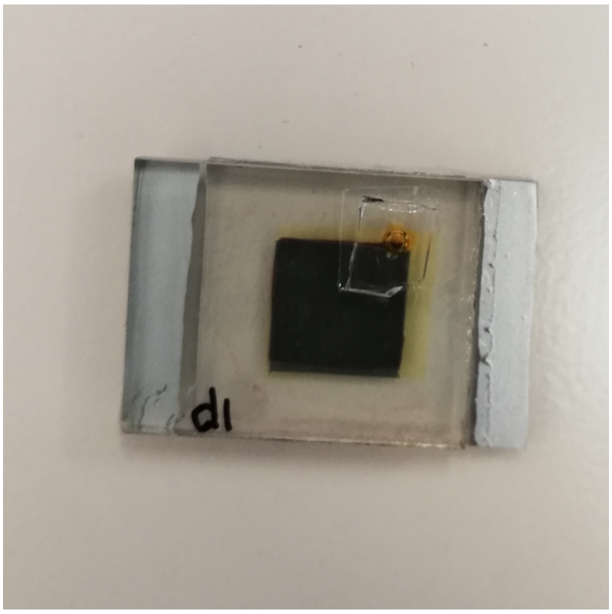

Figure 2.11: Example of one of the fabricated DSSCs (notice that a conductive silver paste has been deposited at the contacts in order to improve the conductivity of the cell)

of deposited titania after the sintering step is 1.57 mg, while the average amount of absorbed dye is 320 μg. Both amounts may be taken under control during the fabrication. In fact, the weight of the TiO_2 layer depends on the amount of paste which is used to perform the coating, while the quantity of dye which covers the semiconductive nanostructured layer relies on the amount of time in which the photoanodes are soaked into the dye. In particular, for longer soaking times, the dye loading will be higher, namely a better coverage of the dye molecules on the TiO_2 nanoparticles is get. However, this does not imply better performances of the device in terms of short circuit currents or efficiencies [17].
Keeping in mind these considerations, we can now characterize the cells in order to evaluate their performances. We perform an IV measurement, like the one explained in the previous section, in such a way to have an estimate of the main parameters characterizing the DSSCs under test. The illumination is provided thanks to a sun simulator and the following IV characteristics are obtained.

By looking at figure 2.12 and table 2.4 it is possible to have an idea of the performances of the device. As we can observe, a quite high density current has been achieved, together with the open circuit voltage. However, the cell behaves in a quite resistive way, as we can se by looking at the fill factor. The reason for this can be related to the fabrication process followed for its production. By the way,

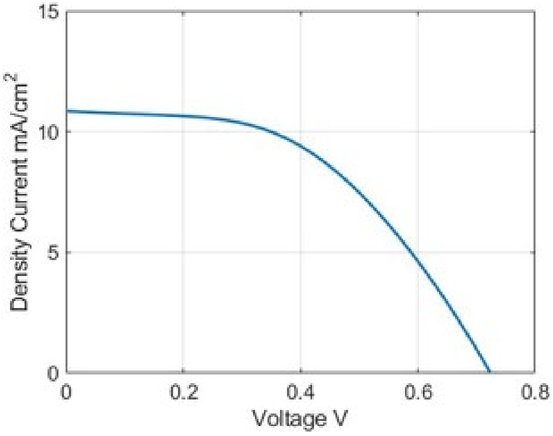

Figure 2.12: IV characteristic for a DSSC

Table 2.3: Parameters describing the performance of the cell

J_{sc}	10.89 mA/cm^2
V_{oc}	0.72 V
FF	0.49
η	3.85 %

comparing our cell with literature, we can notice a quite similar behaviour [fig. 2.13].

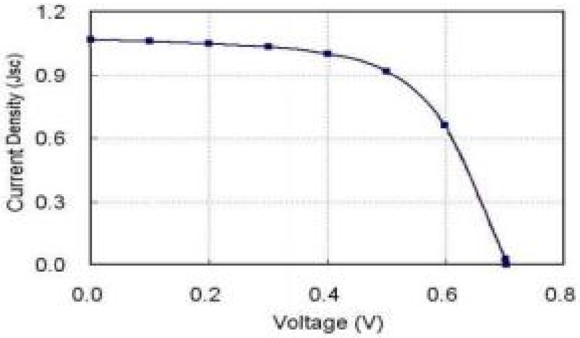

Figure 2.13: IV characteristic from [18]

By looking at the above results, we observe that the maximum open circuit voltage that can be retrieved is limited to a value close to 0.7 V.

Table 2.4: Parameters describing the performance of the cell [18]

J_{sc}	$11.52\ mA/cm^2$
V_{oc}	0.70 V
FF	0.61
η	4.47 %

As previously introduced, this V_{OC} value is too low for the power supply of an external device, which usually needs a voltage of at least 2V. To this purpose, let us consider a series connected module of multiple cells.
According to literature, two different configurations have been proposed for the fabrication of a solar module: the W-type and the Z-type.

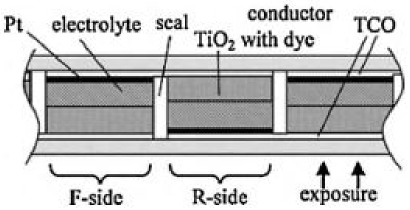

Figure 2.14: Design scheme of W-type serial DSC module [19]

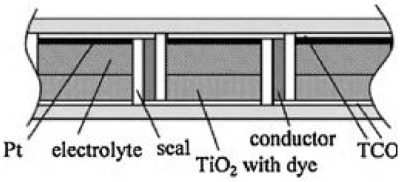

Figure 2.15: Design scheme of Z-type serial DSC module [19]

The Z configuration is characterized by two different electrodes, one hosting all the photoanodes and one hosting all the counter electrodes. Neighbouring cells require interconnections, which are provided by a conductive medium. Here in the following, we will use the silver paste "Silver conductive RS 186-3600", which has to be separated by the active area of the cell through a sealing barrier, in such a way to protect it by electrolyte. In this way, each cell forms a closed chamber where photocurrent can be generated. On the other hand, the W-type configuration does not require any interconnections between adjacent cells since they are alternate bias. This implies an alternation of counter electrodes and photoanodes on the electrode, meaning for instance that for a module with three cells, one electrode will contain two photoanodes and one counter electrode and viceversa for the other one. To be clear, figure 2.16 shows a picture of the module fabricated with a W-type configuration, where the sintered Titania paste for the photoanodes (before the dye soaking) and the sputtered Platinum for the counter electrode are evident. However, also in this case the separation between cells has to be granted, as well as the incisions, so that to allow a correct path for the current.

Since our aim is to create a bifacial-tandem dye-sensitized solar module where a

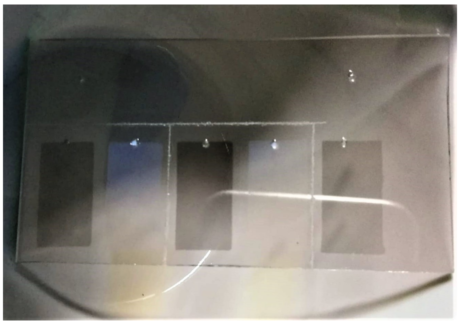

Figure 2.16: Electrode for the W-type configuration, before dye soaking and cell assembly

sharing of the counter electrode occurs, the choice for the best configuration falls to the Z-type.

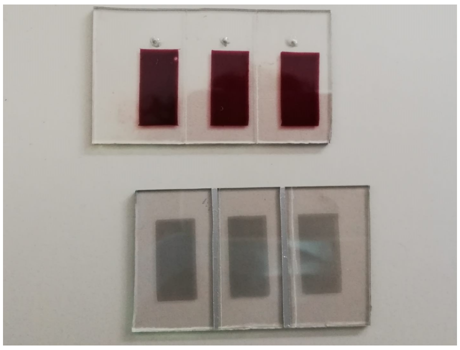

Figure 2.17: Counter electrodes and photoanodes for the Z-type module

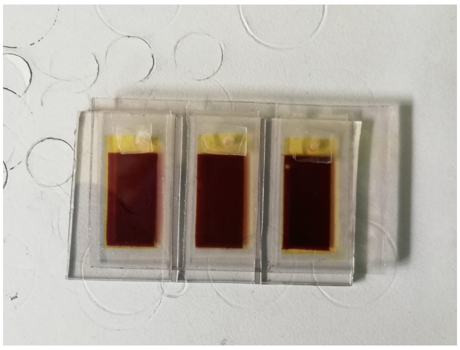

Figure 2.18: Final module after the sealing and the injection of the electrolyte

In figures 2.17 and 2.18 we can observe the design of our module. The experimental procedure for its fabrication is almost the same exploited for the standard single DSSC, with the difference that here interconnections are required. At first, both electrodes have to be engraved with a diamond cutter and then the silver paste (silver lines between cells in figure 2.18) is deposited with a Doctor Blade technique. This allows to crate a path for the current, in such a way that a series connection between the cells occurs. Another difference with respect to the single cells analyzed before concerns the Pt counter electrode [2]. Since we want to exploit

---

[2] Another difference with respect the cell fabricated before consists in the choice of the glass electrode. At first, as mentioned in the experimental section, we used the so called TCO22-7,

the bifaciality properties in the next section of this thesis, the counter electrode has to be transparent. To this aim, the platinum sputtering time has been reduced from 80s to 10s, so to reach a quite good level of transparency.
At this point, we can proceed with the characterization of the module, performed with an IV measurement and with the illumination provided by the solar simulator. Actually, two different modules (we will call them A and B) have been prepared for the experiment. In this way, we will able to simulate the bifacial-tandem structure in the following by simply joining their counter electrodes.

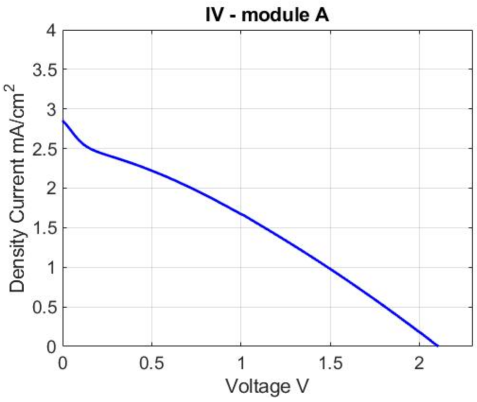

Figure 2.19: IV characterization of module A

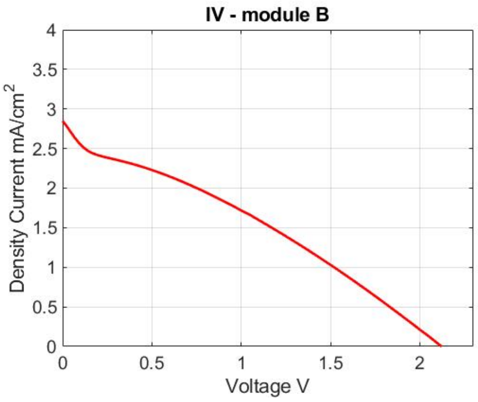

Figure 2.20: IV characterization of module B

Figures 2.22 and 2.23 show respectively the IV characteritics of module A and B. From them, we can extrapolate the main parameters describing the performances of a dye-sensitized solar cell.

By looking at table 2.5 we can discuss the performances of the two modules. At first glance, it is possible to notice that both devices behave more or less in the same way, since they have been fabricated at the same time and following the same steps.
In particular, the module is composed by three different DSSCs connected in series. Each cell has an active area of 2 cm^2, therefore the overall active surface sensitive to the incoming radiation is of 6 cm^2. However, despite the big area, the qualities of the proposed modules are not so good. This can be deduced by looking at the fill factor. It gives an idea of the maximum power with respect to the theoretical power that can be achieved and it is quite low. This can be explained by simply looking

---

from Solaronix. Now we use another product from Solaronix, labeled as TCO16-15. Therefore our electrode is characterized by a thickness of 1.6 mm and by a sheet resistance of 16 ohm/sq.

Table 2.5: Characterization parameters for module A and B

	Module A	Module B
Active area [cm^2]	6	6
$V_{oc}[V]$	2.11	2.12
J_{sc} [mA/cm^2]	2.84	2.83
I_{sc} [mA]	17.04	16.98
FF	0.28	0.29
η [%]	1.69	1.76
P_{max} [mW]	9.99	10.49

at the shapes of the curve, from which we can assume a quite resistive behaviour of the device. An explanation for this can be given by considering the method used for the cells interconnections. The silver paste deposited between the single DSSCs has probably increased the resistance to which the current is subjected during its path in the series connected module. Therefore, the performances of devices are quite poor. This is also enhanced by the obtained values of the efficiencies: η is, in both cases, quite low. Anyway, the silver conductive medium is not the only cause for the bad performances. During the fabrication steps, there are many occasions in which the device could worsen final result. At first, waste survived to the cleaning could be present on the surface. Then, the titania paste could be deposited in a wrong way as well as the soaking in the dye.

However, despite all these improper results, there is still a good one that deserves to be highlighted. If we look at the open circuit voltage, we notice that is very different from the standard ones to which we were used to. For a single cell we usually get a value close to 0.7 V, while here it is more or less tripled. With this series connected module a V_{oc} of almost 2.1 V is obtained, perfectly matching what we expected. Since three different cells are placed in the same device, the open circuit voltage of a single one has to be multiplied by the total amount of cells. Therefore the experiment, at least for what concerns this last parameter, has led to a very good outcome.

The reason for which we fabricate a module instead of a single cell is, as already said, to reach a device that can give an output suitable for the power supply of an external device, like a sensor for instance. As introduced before, these kind of devices requires a voltage of at least 2 V, therefore we can conclude that a dye-sensitized solar module composed of three cells satisfy the requirement that we have. On the same way, we can also say that, increasing the amount of cells integrated in the same module, higher open circuit voltage can be obtained and therefore higher power can be supplied.

2.5 1st optimization: the design

As already mentioned in the introductory chapter, a standard dye sensitized solar cell, like the ones studied in the previous section, can be optimized in order to improve its output. In particular, we would like to create a device which can minimize the incoming radiation losses, leading thus to a better absorption and therefore to finest efficiencies.
The idea is the one already shown in figure 1.5, where both bifacial and tandem properties are combined in a unique device.

According to literature, a bifacial DSSC is a cell able to receive light from both sides, photoanode and counter electrode. This last has to be necessarily transparent in such a way that the incoming radiation can reach the photactive area of the system. In fact, with a combined front and rear illumination, more dye molecules are excited and more carriers are generated. The result is the enhancement of short-circuit current density and therefore of the overall conversion efficiency. Of course, the photogenerated current will be lower when we consider the rear illumination only (light directly on the counter electrode), since the higher reflectivity and the larger distance from the anode, the place where the photosensitive element is located. On the other hand, when the radiation hits the photoanode, a better response is recorded.
Let us now consider what a tandem DSSC is. As introduced before, a standard solar cell is intrinsically related to the concept of losses. When under illumination, the cell is not able to adsorb all the incoming radiation, leading to a degradation of the photon to electron conversion efficiency. To this purpose, tandem solar cells have been proposed in last years. They can be thought as individual cells with different bandgaps stacked one on top of the other, in such a way that photons which are not adsorbed by the first stack, can be collected by the following ones. The idea behind the tandem structured dye-sensitized solar cells allows to take full advantage of the incoming radiation, effectively broadening the absorption spectrum of the cell, resulting in a higher open circuit voltage or short circuit current with respect to the conventional DSSC with single light absorber.

At this point, let us combine both bifacial and tandem properties of solar cell in such a way to retrieve a new design able to provide improved results. In particular, what we expect is to obtain a cell that can be both front and rear illuminated and at the same time presents a vertically stacked structure to increase the absorption.

In figure 2.21, a first tentative of bifacial-tandem DSSC is proposed. Before taking into account the performances obtained with the characterization techniques described in the introductory part, let us focus on the structure of the cell.

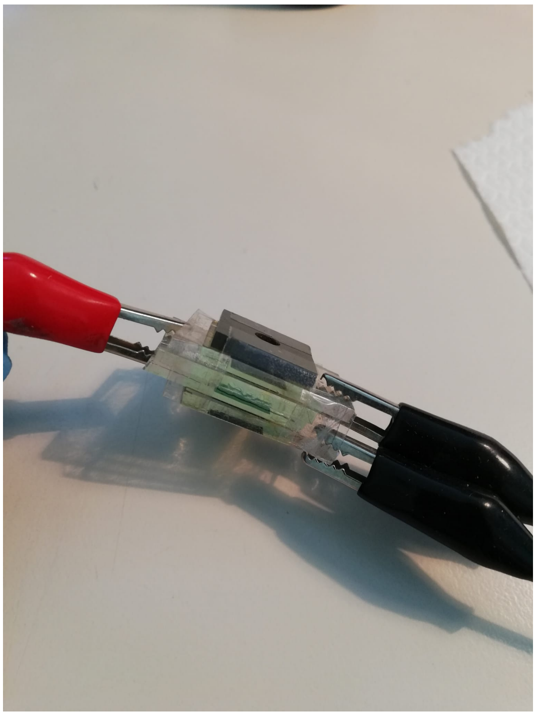

Figure 2.21: Side view of bifacial-tandem dye-sensitized solar cell

As we can observe in the figure, the device is composed by two different counter electrodes that are sandwiched between two different photoanodes. The device is in fact obtained by simply putting in contact the counter electrodes of two single solar cells.
To this purpose, an important requirement must be respected for the fabrication of the counter electrodes: they have to be transparent. In fact, we want that the light which is not absorbed by the first photoanode, the one who faces the incoming radiation, can be absorbed by the underlying one. To obtain this effect, the counter electrodes have to be not opaque in such a way that the radiation can be transmitted through them. This result can be achieved by simply reducing the Platinum sputtering time to which the electrode is subjected: instead of 80s we reduce the time to 10s and transparency is get.
At the same time, we realize a cell which has a transparent photoanode too. To this aim, we utilize a titania paste from Solaronix: Ti-Nanoxide T/SP. It is characterized by highly dispersed titania nanoparticle paste, suitable for the deposition of transparent active mesoporous layers. Then, the sintered films feature a very high surface area ensuring efficient dye loading.

Once that both counter electrodes and both photoanodes have been fabricated, the

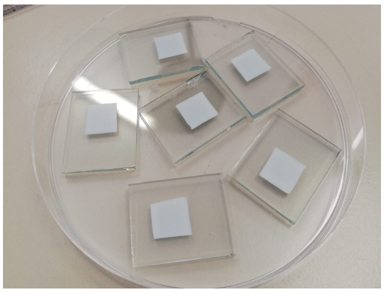

Figure 2.22: Photoanode with opaque D/SP titania paste after sintering

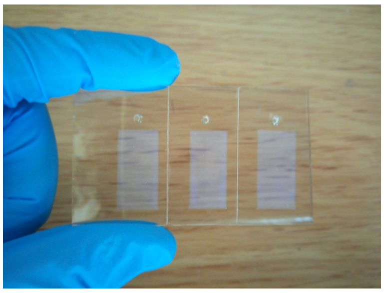

Figure 2.23: Photoanode with transparent T/SP titania paste after sintering

two single cells can be assembled following the same steps illustrated before.

2.5.1 Results and data analysis

Let us characterize our bifacial-tandem solar cell with the IV measurement explained before. In particular, we perform an analysis on a bifacial-tandem cell composed by two different cells, which are put one on top of the other in such a way that their counter electrodes touch each other. Moreover, we perform the characterization by illuminating first the front cell and then the rear one [fig. 2.24].

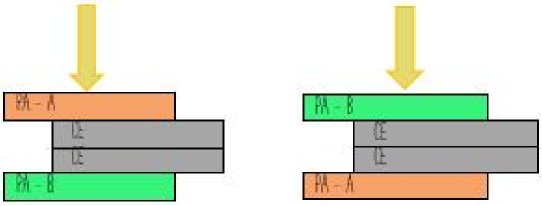

Figure 2.24: Picture describing the assembly of a bifacial-tandem solar cell

At this point, we are ready to characterize the bifacial-tandem dye-sensitized solar cell, illuminating at first photoanode A and then the B one.
By looking at the obtained data, interesting aspects can be highlighted.
Let us consider at first the open circuit voltage. As we can see, we achieve again a V_{oc} close to 0.7 V. Since for a bifacial-tandem solar cell, the two cells are connected in parallel, we expect no changes in this value, view that a parallel connection

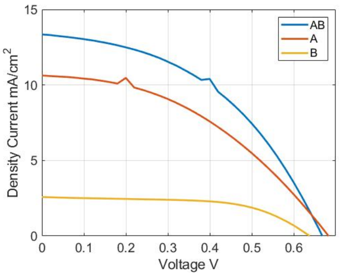

Figure 2.25: IV characteristic of the cell by illuminating photoanode A

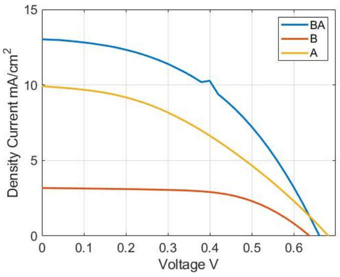

Figure 2.26: IV characteristic of the cell by illuminating photoanode B

Table 2.6: Characterization parameters related to figure 2.25

	AB	A	B
$V_{oc}[V]$	0.67	0.68	0.64
J_{sc} $[mA/cm^2]$	13.34	10.62	2.58
FF	0.47	0.42	0.59
η [%]	4.16	3.03	0.97

Table 2.7: Characterization parameters related to figure 2.26

	AB	A	B
$V_{oc}[V]$	0.66	0.68	0.64
J_{sc} $[mA/cm^2]$	13.03	9.93	3.17
FF	0.48	0.39	0.60
η [%]	4.11	2.66	1.22

implies same voltage values for each element. On the other hand, by looking at the short circuit current densities, we notice that the achieved values are quite higher with respect to the case reported before in table 2.4. This result is consistent with our expectations, since, as we introduced before, the idea behind a bifacial-tandem dye-sensitized solar cell is that the incoming radiation which is not absorbed by the first photoanode can be collected by the underlying one. This means that more photons can be captured by the photo-sensitive element and therefore more electrons will be photo-generated. In addition to this, we can also notice that J_{sc} values are quite close in both cases, illuminating cell A and then cell B. This allows us to say that the bifaciality property can be achieved with this kind of design. In fact, no matter what side we are illuminating, the obtained current is almost the same. The concept of bifaciality is further satisfied by the efficiencies. Also in this case, the values are quite similar, indicating a bifaciality index almost equal to one. Furthermore, η is higher with respect the previous case [tab. 2.4], meaning that tandem properties have been complied too.

At this point, we can proceed as before and fabricate a series connected module in order to achieve higher values of the open circuit voltage. In particular, we use again the already studied modules discussed above and presented in figure 2.18.

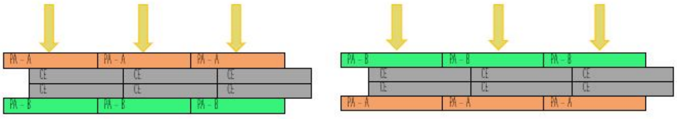

Figure 2.27: Picture describing the assembly of a bifacial-tandem series connected module

To perform the analysis on a bifacial-tandem series connected module we take into account the modules analysed before, putting them one on top of the other with the configuration already exploited: photoanode-counter electrode:counter electrode-photoanode. Moreover, exactly as before, we perform the characterization illuminating at first module A and then module B.

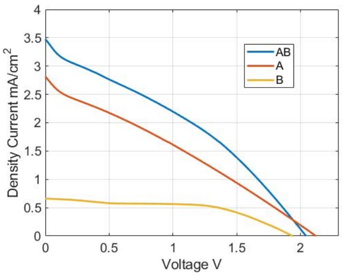

Figure 2.28: IV characteristic of the bifacial-tandem module by illuminating photanode A

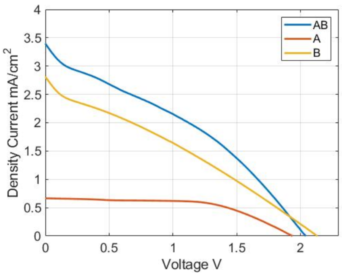

Figure 2.29: IV characteristic of the bifacial-tandem module by illuminating photanode B

Table 2.8: Characterization parameters related to figure 2.28

	AB	A	B
Active area $[cm^2]$	6	6	6
$V_{oc}[V]$	2.04	2.11	1.92
J_{sc} $[mA/cm^2]$	3.42	2.76	0.66
I_{sc} [mA]	20.52	16.56	3.96
FF	0.33	0.28	0.53
η [%]	2.31	1.63	0.68
$P_{max}[mW]$	13.87	9.78	4.3

Table 2.9: Characterization parameters related to figure 2.29

	BA	B	A
Active area $[cm^2]$	6	6	6
$V_{oc}[V]$	2.04	2.11	1.92
J_{sc} $[mA/cm^2]$	3.33	2.74	0.66
I_{sc} [mA]	19.98	16.44	3.96
FF	0.33	0.28	0.58
η [%]	2.24	1.62	0.7
$P_{max}[mW]$	14.71	8.98	4.59

Also in this case we can observe that both bifaciality and tandem properties have been satisfied: the photo-generated currents are increased with respect to the case of one single module and they are quite similar independently from the side which is illuminated. Also the efficiencies reach higher values, in accordance with what said before: view that the incoming radiation which is not absorbed by the first module can be collected by the second one, the photo-generated current will be higher and so does the efficiency.
An other interesting point is related to the values listed for modules A and B. We have tested the performances of the single modules while connected in a bifacial-tandem configuration. This means that, if we consider the module AB (A on the top, B on the bottom), we have at first contact only the module A and then the underlying module B. We observe for this last one that a quite low value of density current is achieved. This is due to the fact that this module is actually covered by A which is the one directly illuminated by the incoming radiation. However, looking at both density currents of A and B, we can notice that their sum is almost equal to the photo-generated current of the bifacial-tandem module. The same behaviour can be observed by considering the efficiencies too. This result is very interesting, since we can say that the parallel connection is working and that the overall performances of the device have been boosted.

2.5.2 Future improvements

Up to now, we have fabricate and then characterized a tandem/bifacial dye sensitized solar module. As mentioned in the introduction, the aim is to have a bifacial module in which the counter electrode is shared by both modules. However, the study here proposed does not present this kind of result, view that the glassy electrodes used for the fabrication of the cells are not conductive on both sides.

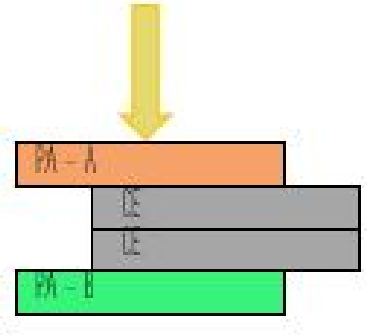

Figure 2.30: Design of the bifacial/-tandem dye sensitized solar module proposed in this thesis activity

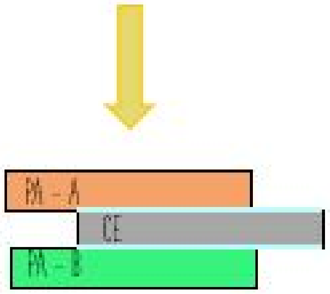

Figure 2.31: Design of the optimized bifacial/tandem dye sensitized solar module

It is evident that design proposed in figure 2.31 is the one that could lead to better results for what concerns the performance of the modules. In fact, if two different counter electrodes are used, the incoming radiation has to cross one more interface with respect the case in figure 2.30. This means that refraction phenomena will occur and less illumination will be provided on the underlying cell.
In order to solve this problem, it could be interesting to find a way to make both sides of the glass electrode conductive. Here we propose same ideas that can be implemented in the future to achieve this result.

- A first solution can be the deposition of a conductive layer on the sides of the electrode which is not conductive. This can be performed by sputtering ITO, namely a thin layer of indium-tin oxide. It is the most employed conductive material which is transparent too, when very thin. View that it is transparent to visible light, a physical vapour deposition of this kind of material can be a good choice to solve our problem.

- Another solution could be to change the material of the electrode. For instance, we can fabricate a flexible design: instead of glass, we can use a transparent polymide electrode with deposition of conductive layers on both sides. This material can support very high temperatures, therefore it could be a good choice if we consider the temperature at which it has to be subjected during the sintering of the titania anode. Moreover, it keeps the transparency properties of the glass and it can be covered by a conductive layer. Also in this case ITO can be a good choice. Nevertheless, instead of a PVD, we can also think to implement a different technique for the realization of a conductive layer. A conductive mesh of silver nanowire passivated with TiO2 can be used, allowing the electrode to be conductive on both side.

2.6 2nd optimization: new materials

At the beginning of this thesis activity, the topic concerning the Internet of Things world has been mentioned. Year by year, the attention of the scientific community is more and more focused on the IoT field and the technological efforts have even more grown up. However, all IoT devices share one common problem: charging is not so easy. Common batteries have been employed for years, but the issues concerning their limited life times and their need to be re-charged let them a not so appropriate choice. It is for this reason that DSSCs have been proposed. View that they are able to generate an electrical current under illumination conditions, they could be the best choice to provide a power supply for IoT devices. Moreover, many research activities, have demonstrated that dye-sensitized solar cells show very good performance under indoor light conditions, letting them to be even better to charge IoT devices which are usually located in our home, where outdoor illumination does not reach. In fact, in most cases, IoT devices require a power supply which is typically quite low and therefore ambient light impinging on a DSSC generates a sufficient amount of power.

Many studies have been carried on in the last recent years in order to find out which are the best materials and the most suitable indoor lighting source to fabricate a DSSC. In particular, it turns out that LED and fluorescent lamps are the most energy efficient light for our everyday lives. In most indoor DSSC cases also displayed the highest efficiency because of their narrower spectral widths without the low-photon-energy infrared emission [20]. At the same time, universities, researchers and the PV industry itself are investigating different photoanodes, counter electrodes, sensitizers and electrolytes in order to create a cell which can achieve very high performances under ambient light. However, very few publications can be found in literature regarding the performance under such conditions. Moreover, the few existing reports all describe dye-sensitized solar cells based on iodide electrolytes in combination with a ruthenium dye.

One of the first tentative in which other materials where tested occurs in 2005, when Fukuzumi and co-workers tried to substitute iodide with copper complexes, finding out that it worked well as redox mediators at reduced light intensities [21]. In this occasion, Fukuzumi et al. discovered that for a DSSC based on $[Cu(dmp)_2]^{2+/+}$ electrolyte, under the weak solar light irradiation of 20 mW/cm^2, values of efficiency close to 2.2% were achieved. It is still a quite low value and especially lower with respect to the one obtained for a iodine-based electrolyte, but the turning point is given by the open circuit voltage that can be reached.

Figure 2.32 exactly demonstrates what just said. Changing the electrolyte from a iodine-based one to a copper-based one, does not improve the device in terms of performances, but on the other hand allows to reach higher values of V_{oc}, therefore

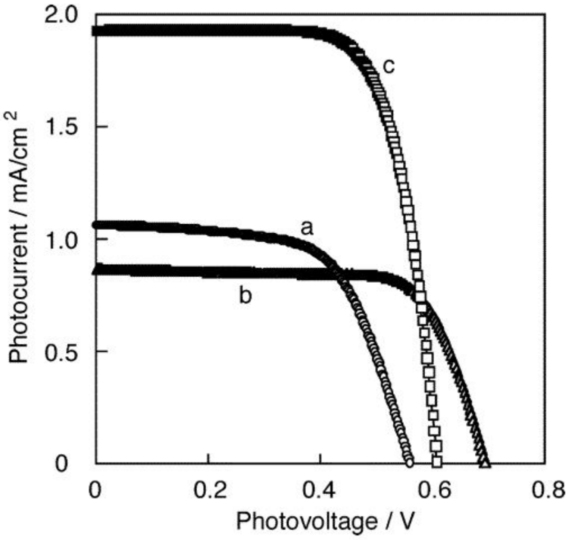

Figure 2.32: IV curves of DSSCs using (a) $[Cu(SP)(mmt)]^{0/-}$, (b) $[Cu(dmp)_2]^{2+/+}$, and (c) I_3^-/I^- as the redox couples; input power: 20 mW/cm^2 [21]

increasing the possibility for the power supply of IoT devices.

After Fukuzumi, many others tried to investigate new materials for the production of indoor DSSCs. One of them is Hannes Michaels that, with his co-workers, published in 2020 a paper explaining the benefits of copper-based electrolytes for dye-sensitized solar cells under ambient light [22]. The research activity was not focused only on the investigation of the electrolyte, but even on the choice of the sensitizer.

We dedicate the following sections of this chapter to investigate and reproduce the work proposed by Michaels et al., in such a way to fabricate a new kind of solar cell. We expect to reach higher open circuit voltage because of the presence of the copper-based electrolyte and higher short circuit current coming from the co-sensitization of two different dyes.

2.6.1 Experimental section

The aim of this section is to fabricate dye-sensitized solar cell reproducing the one fabricated by Michaels et al. in [22]. By taking this paper as reference, the following fabrication process has been implemented.

For the electrodes shaping, cleaning and photoanode production, the steps are the same already explained in the previous section when a standard DSSC was tested. Therefore a TiO_2 nanoparticles paste is Dr. Bladed on a FTO electrodes and then

sintered at 450 °C. Even the process for the electrolyte injection and for the cell assembly stays the same: a hole is drilled on the surface of the electrode to allow the filling of the chamber with the electrolyte and a thermoplastic film is used for the sealing. Differently form what was done in [22], also the counter electrode is made by us with the same material exploited in previous sections. In literature, they used a PEDOT-based counter electrode, while in the following we will use Platinum as usual. Unfortunately, PEDOT was not commercially available in our laboratory, therefore Pt was tried, together with other alternatives that we will describe successively.
Now, the innovative part: the electrolyte and the sensitizer.

Sensitizer:
The dye proposed in literature is composed by the co-sensitization between XY1 and L1, in a ratio 1:2.5. In particular, the first one is made by a concentration of 0.1 mM of XY1 together with 1mM of chenodeoxycholic acid (CDCA) in a solution of chloroform and ethanol in a ratio 3:7. Actually, we will use isopropanol instead of chloroform, because of the toxicity of this last solvent. For what concerns the other dye, it is composed by a concentration of 0.5 mM of L1 dissolved in acetonitrile.
For the production of the co-sensitization of the two different dyes, we use a falcon of 50 ml. Therefore, in order to keep the ratio 1:2.5 imposed by the paper, we need 14.3 ml of XY1 and 35.7 ml of L1.

Table 2.10: XY1 and L1 dye components

Material	Quantity
XY1	2.31 mg
CDCA	5.61 mg
Isopropanol + Ethanol	4.29 ml

Material	Quantity
L1	7.54 mg

Electrolyte:

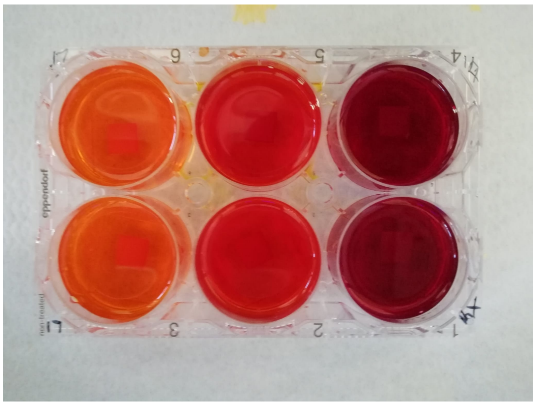

Figure 2.33: From left to right: L1 - XY1:L1 - XY1

For the electrolyte we need: 0.2 M of $Cu(tmby)_2TFSI$, 0.04 M of $Cu(tmby)_2TFSI_2$, 0.6 M of 4-tert-butylpyridine in acetonitrile solution and 0.1 M of LiTFSI.

Table 2.11: Electrolyte components

Material	Quantity
$Cu(tmby)_2TFSI$	1.536 g
$Cu(tmby)_2TFSI_2$	419 mg
4TBP	811 mg
LiTFSI	287 mg

2.6.2 Results and data analysis

At this point, we are ready to characterize the device. An IV measurement is performed exactly as we did for previous standard cells.

Table 2.12: Parameters describing the performance of the analysed cell

J_{sc}	5.28 mA/cm^2
V_{oc}	0.97 V
FF	0.42
η	2.15 %

Before commenting the obtained results, let us compare the cell characteristics with those obtained by Michaels et al. in [22].
By looking at figures 2.34 and 2.35 we notice that different results are obtained. In particular, smaller values of both short circuit current and efficiency are achieved.

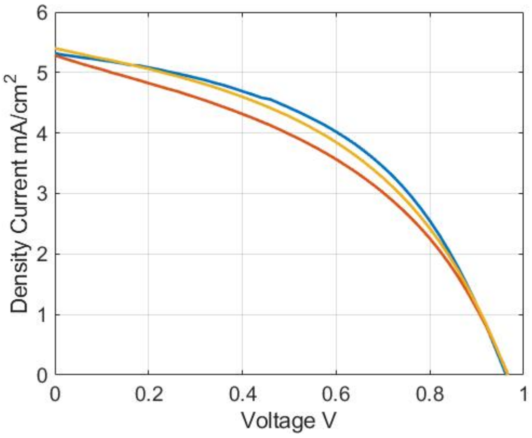

Figure 2.34: IV characteristic for a dye-sensitized solar cell with copper-based electrolyte and XY1:L1 co-sensitizers

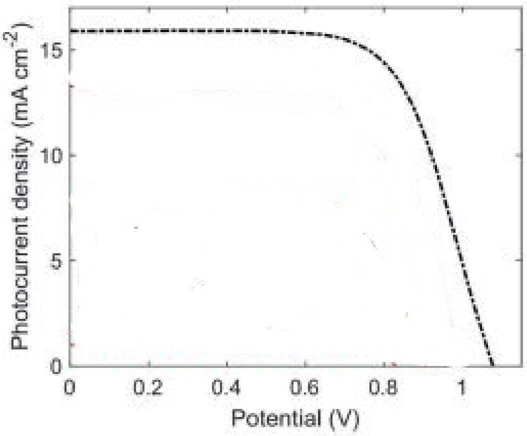

Figure 2.35: IV characteristic for a dye-sensitized solar cell with copper-based electrolyte and XY1:L1 co-sensitizers from [22]

Table 2.13: Parameters describing the performance of the cell proposed in [22]

J_{sc}	15.9 mA/cm^2
V_{oc}	1.08 V
FF	0.67
η	11.5 %

These discrepancies can be justified by the process used for the fabrication of the cells (see table 2.14).

Table 2.14: Materials employed for the fabrication of the device

	Literature	First cell
Current collector	FTO	FTO
Porous semiconductor	TiO_2	TiO_2
Dye	XY1+L1	XY1+L1
Electrolyte	Cu-based	Cu-based
Counter electrode	PEDOT	Pt
Treatment	$TiCl_4$	None

From this, we can deduce that using a Platinum counter electrode is not a proper choice for this kind of device. According to literature [23], Li et al. observed that in an electrochemical cell composed by Platinum counter electrode and Cu-based electrolyte, the reduction process was relatively slower when compared to oxidation. In fact, the redox potential of the copper complex was found to be 0.97 V which is far more positive than that of the I^-/I^{3-}. Therefore, a lower reduction rate implies that oxidation occurs more frequently, meaning an incompetent catalytic activity between Platinum and copper redox mediators. This was even visibly evident on the aspect of the cell after few days from the assembly: the color of the Pt counter electrode, in contact with the Cu electrolyte, changes at sight revealing an oxidation process.
Moreover, even the absence of a post-treatment, like the one performed in literature with $TiCl_4$, implies worst results. A post-treatment like this leads to an increase of the size of TiO_2 nanoparticles allowing an improvement on the electrons transfer path on the TiO_2 layer. Moreover, $TiCl_4$ helps in the suppression of the charge recombination between TiO_2 and the electrolyte interface: it increases the charge transfer resistance. Finally, it leads to better electrons lifetime implying an enhancement of charge collection efficiency [24].

However, we have not mentioned yet a good result that we have achieved. Despite the bad performances of our cell, an interesting point lies in the open circuit voltage. In fact, here we get a $V_{oc} = 0.97V$, definitely higher than the one usually obtained with a standard DSSC (iodine-based electrolyte and N719 dye).
According to literature [25], an enhancement of the open circuit voltage corresponds to a boost of the overall performances of the device and this can be performed by properly selecting the redox mediator. Since, the V_{oc} arises from the difference between the quasi-Fermi level position in the semiconductor photoanode and the energy level corresponding to the redox potential of the mediator, to increase the open circuit voltage we can both upshifting the potential of the redox mediator or downshifting the Fermi level of the photoanode. For the first strategy, Cu-based

redox shuttles provide good results since it exhibits an extremely positive potential (0.97 V). On the other hand, to lower the Fermi level of the semiconductor, 4TBP can be added to the electrolyte. This additive implies significant slowdown of electrode kinetics and diffusion rate, leading to the desired Fermi level shift and to a decrease of the electron recombination [25].
Beside the electrolyte, even the sensitizer has a role in the improvement of the performances of the cell and in the increasing of the open circuit voltage itself. In fact, L1 has a large electronic transition energy which implies a huge injection of high-energetic electrons into the conduction band of the semiconductor covering the photoanode [22]. This contributes to upshifting the Fermi level, leading, as mentioned before, to an increase of the V_{oc}.
This last is not the only contribution brought by the dye. At first, we have to take into account that we are not using a single dye, but instead the co-sensitization of two photo-sensitive elements is performed. In particular, because of their different sizes, these molecules can reach a very good TiO_2 surface coverage. Since L1 molecules are quite smaller than XY1 ones, L1s can occupy the interstices between larger XY1s (see figure 2.36).

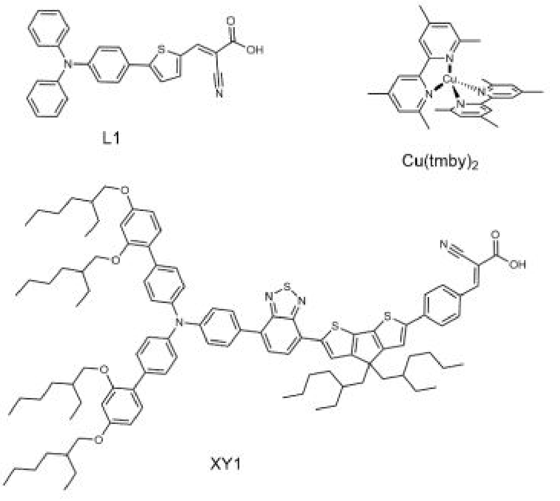

Figure 2.36: Chemical structures of investigated dyes L1, XY1 as well as copper redox mediator $Cu(tmby)_2$ (from supporting information of [22])

The complementary activity of XY1 and L1 operates on the light absorption too. A boost in the photon collection can be achieved leading to an increase of electrons which are injected in the semiconductor conduction band. Since a large number of photons can be absorbed, we expect that the photo generated current will increase too. In fact, according to literature [22], the co-sensitization of these two different dyes should lead to higher short circuit currents. However this result is not achieved

by our experiment.
To explain this last discrepancy, we have performed an analysis on XY1 and L1 separately and then on their co-sensitization.

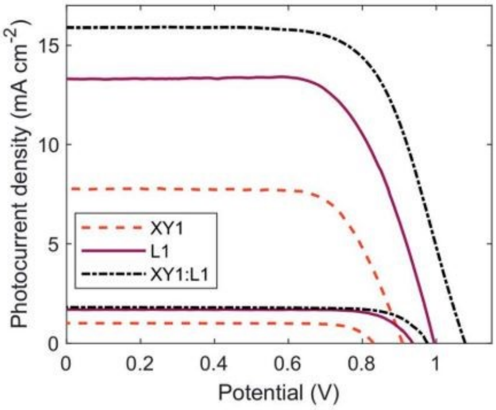

Figure 2.37: Behaviour before and after the co-sensitization according to literature [22]

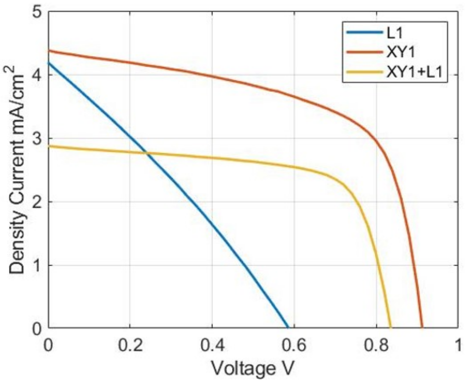

Figure 2.38: Behaviour before and after the co-sensitization according to our experiment

It is evident that the achieved results are not satisfactory at all. Not only the dyes before the co-sensitization do not behave as expected, but even their co-sensitization leads to worst results. It is like if the co-sensitization damages the effect of the dye inside the cell.

Table 2.15: Relevant parameters for the different dyes according to [22]

	XY1	L1	XY1:L1
$V_{oc}[V]$	1	0.91	1.08
$J_{sc}\ [mA/cm^2]$	13.3	9.4	15.9
FF	0.67	0.71	0.67
η [%]	8.9	6.1	11.5

Table 2.16: Relevant parameters for the different dyes according to our experiment

	XY1	L1	XY1:L1
$V_{oc}[V]$	0.91	0.58	0.84
$J_{sc}\ [mA/cm^2]$	4.37	4.19	2.87
FF	0.61	0.29	0.69
η [%]	2.43	0.71	1.65

Tables 2.15 and 2.16 are a further proof of what just said. According to our experiment, the co-sensitization does not work. As well as we did for the previous discording results, we can blame the choice of the counter electrode. We have demonstrated once again that Platinum is not suitable with this kind of materials since it tends to oxidize reducing the performances of the system.
Despite all these inconsistencies, one last experiment wants to be reproduced from the paper of Michaels et al. They have found out a new interesting behaviour of their Cu-based cells. In particular, they have noticed that after few times, the

electrolyte based on copper tends to evaporate leaving a solid residual inside the chamber where redox phenomena occur. Nevertheless the liquid solvent is not present anymore, the solid Cu particles are sufficient for the correct working of the dye-sensitized solar cell. They address this new behaviour to the so called "Zombie cells", named like this since they work even if the redox mediator responsible for the electron transport is not present as it was before the evaporation. It is a quite incredible discovery, since in practical applications solar cells have to survive to harsh conditions, operating in several range of temperature, humidity, etc. that could effectively cause the evaportation of the electrolyte.

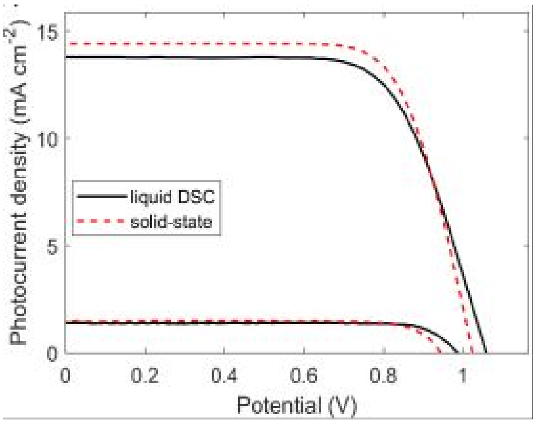

Figure 2.39: IV characteristic of the zombie cell proposed in the supporting information of [**21**]

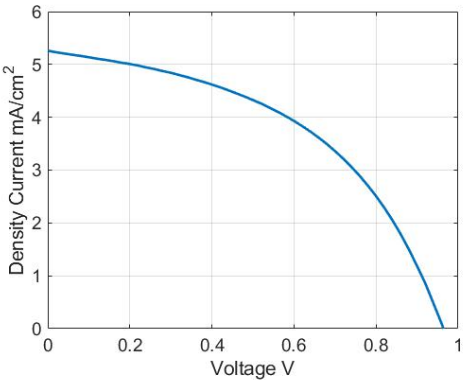

Figure 2.40: IV characteristic of the zombie cell after one day from the fabrication

To better appreciate what shown in figure 2.40, let us list the relevant parameters characterizing the zombie cell.

Table 2.17: Parameters describing the performance of the zombie cell

J_{sc}	5.11 mA/cm^2
V_{oc}	0.97 V
FF	0.44
η	2.19 %

If we compare table 2.17 with table 2.12 we can notice that none of the parameters has changed too much. Therefore, we can conclude that the solid residual electrolyte survived after the evaporation is sufficient for a correct working of the cell.

From all the previous analysis we have find out many times the incompatibility of Platinum as material for the counter electrode. To this aim, other materials have been tested, since the impossibility to employ PEDOT as suggested by Michaels and co-workers. In the following, we propose several EIS measurements with the goal to investigate the charge transfer resistance of different materials, namely the resistance at the electrode/electrolyte interface. In fact, this last parameter could be considered as the responsible for the lower reduction rate of Pt mentioned before.

To perform this analysis, a symmetric cell has been fabricated exploiting a microfluidic housing system like the one in figure 2.41.

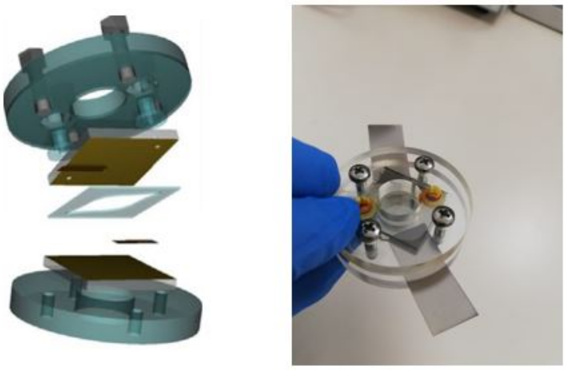

Figure 2.41: Set up for the microfluidic housing system [26]

This kind of cell holder allows the investigation of the components of the cell since it can be opened and closed as we desire. In particular the system is composed by two holder which sandwich two equal electrodes. The material to investigate is deposited on both FTO electrodes and the Cu-based electrolyte is injected between them. In order to confine the electrolyte in the region of interest and to maintain the control on the active area, a PDMS membrane is exploited. In fact, the PDMS polymer allows a good level of transparency, together with low costs and simple processability.

At this point, let list the materials that we will investigate.

- Platinum: deposited with sputtering (30mA/10s);
- Graphite: deposited with 6B pencil-lead;
- PEDOT:PSS: deposited with spin coating.

Performing an Electrochemical Impedance Spectroscopy with respect to the OCP, the following results are achieved.

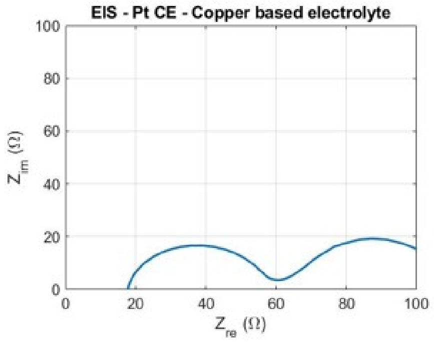

Figure 2.42: EIS for a microfluidic housing system hosting Platinum electrodes

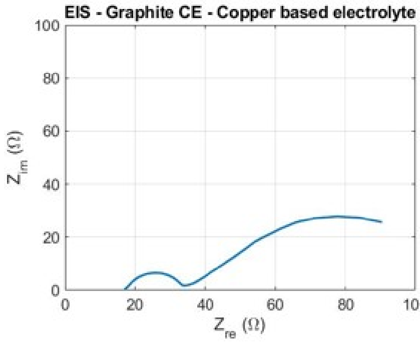

Figure 2.43: EIS for a microfluidic housing system hosting graphite electrodes

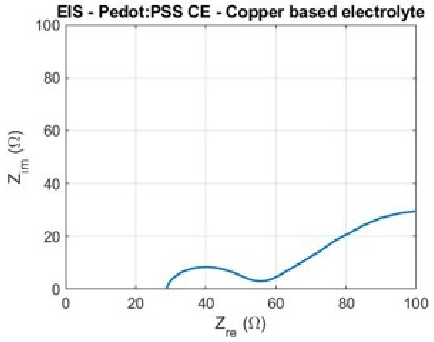

Figure 2.44: EIS for a microfluidic housing system hosting PEDOT:PSS electrodes

In order to have a clear interpretation of the obtained plots, let us evaluate the values of both series resistance and charge transfer resistance.

Table 2.18: Series resistances and charge transfer resistance for different materials

	R_s [Ω]	R_{ct}[Ω]
Pt	17.741	21.4152
Graphite	17.086	8.695
PEDOT:PSS	28.7309	13.6983

Interesting results can be read from the above table and figures. As expected, Pt shows quite high values of charge transfer resistance, consistent whit was expected. However, it is not the worst material that we tested: PEDOT:PSS leads to even more bad results. This material is the mixture of two ionomers, one is made up of sodium polystyrene sulfonate which is a sulfonated polystyrene, while the other is PEDOT. Even if this last is the material used by Michaels et al. in their experiments, the presence of the sulfonated dopant prevents to achieve good performances. In some way it interacts with the electrolyte in a non proper way, damaging the overall performances.

On the other hand, graphite seems to be the material most suited for the counter electrode. It shows a quite low R_{ct} and therefore we could think to implement it in the fabrication of a new cell which exploits both Cu-based electrolyte and XY1-L1 dye. However, the process used for its deposition is not so reproducible and efficient. In this case, electrodes have been just painted with a 6B pencil, made of course of graphite. This handmade technique does not allow a good control of the thickness of the deposited layer as well as it does not allow to reach a proper level of transparency. More sophisticated techniques should be employed (see next section 2.6.3 for future improvements that we can introduce in this system).

2.6.3 Future improvements

In the previous section we have observed that not so good results were obtained if compared to the one reported by Michaels et al. Therefore, here we want to propose some possible improvements that can be implemented for the production of this kind of solar cell.

- Of course, the first trial lies on the choice of the counter electrode. We have seen many times that Platinum does not work so well because of its low reduction rate when in contact with a copper based electrolyte. The most suitable choice would be to use a PEDOT counter electrode, like the one exploited in literature. To this aim, it would be interesting to work with both a commercially available PEDOT material and also with EDOT, trying to perform its electro-polymerization in order to achieve the final element that we need.

- Another possibility relies on the investigation of carbon based materials. We have observed that graphite could be a good choice, but a reproducibility for what concerns its deposition is required. To this aim, we can exploit a PVD technique, like sputtering, where a target of graphite is physically bombarded in such a way to have a deposited layer on our sample.

- Post-treatment. It could be useful to perform a post-treatment of the electrode. One possibility could be to use $TiCl_4$ as done by Michaels et al. However, we could also exploit the deposition of a blocking layer in order to reduce recombination effects that damage the performance of the device.

- Let us think at the bifacial/tandem DSSCs investigated during the course of this thesis activity. It will be interesting to fabricate them with these new materials proposed in this section. If we would able to produce a module based on XY1:L1 and copper redox mediator, then higher open circuit voltage can be achieved, together with higher efficiencies. The only foresight of this application is the need of transparency. For bifacial/tandem cells, all the system needs to be transparent as much as it can, in order to allow the transmission of the incoming radiation between the different cells. To this aim, it could interesting to try a diluted Cu-based electrolyte to improve the transparency.

- Finally, always to investigate the transparency of the system, it could be interesting to conduct a transmittance analysis of both Cu-based and I-based electrolytes, in such a way to exploit their transmission properties.

Chapter 3

Supercapacitor

Up to now we have focused our attention on the fabrication and characterization of a solar module, responsible of the energy harvesting of the device that we want to produce at the very end of this thesis. Along with this, we are also interested in the storage part, namely we need a device able to store the energy photo-generated by the DSSC.

Nowadays battery technology is well known and consolidated in the scientific community, but many drawbacks affect its performances. Lower life-cycle, less power density, higher charging time, heating and environment problems force to find new alternative solutions. Here in the following we propose the supercapacitor as a device able to replace the battery in a storage system. A supercapacitor (SC) is an electrical energy storage system similar to the conventional capacitor, but with much higher capacitance values and energy density. It behaves in a way that combine both batteries and capacitors properties into a single device, with very smaller charging time and discharge behaviour like a regular battery. SCs are comparatively more expensive, but they provide high energy storage with low equivalent internal resistances (suitable for high power applications), and fast charge/discharge switching.

Depending on the working principle, they can be split into different capacitors:

- **Electrical double layer capacitance (EDLC)**. The electrical energy is stored thanks to the Electric Double Layer (EDL) formed at the interfaces between electrodes and electrolyte [fig. 3.1]. When a voltage is applied the electrodes gain positive or negative charge, and a layer of opposite charges clusters on the interface between the electrodes and the electrolyte. Since the amount of charge stored in the EDL is proportional to the electrode surface, Activated carbon (AC) is used for the active component of the electrode, which provides high surface area.
- **Pseudo-capacitance**. Energy is stored thanks to faradaic redox reactions at

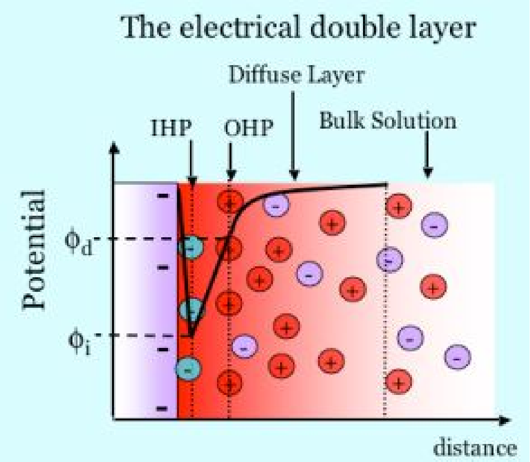

Figure 3.1: Schematic representation of an Electrical Double layer [[27]]. A potential (called Zeta potential) is formed at the surface of the electrode, and two adjacent layers of charge build up in the electrolyte: the Stern layer (typical length in the order of some Angstrom), and a diffuse layer of mobile counter-ions.

the surface of the electrodes, along with the creation of static EDLs. In this case, electrodes are characterized by metal oxides or conductive polymers, in order to enhance fast reversible surface reactions. The main difference with batteries is that the reactions occur only along the surface of the electrode, and not in the bulk (faster process).

For what concerns the EDL SCs, they provide high power density with great cycling stability; this is an important feature, since the electrodes do not get damaged in the cycling process. In the other hand, since carbon materials are widely used as active materials for the electrodes, high capacitances can not be achieved. Pseudo-capacitors reach higher capacitance, but they experience lower electrical conductivity and poorer rate capability (because of the redox reactions that may damage the electrodes).
As already introduced in the beginning, a general Ragone chart provides a good comparison of the energy densities for various energy-storing devices [fig. 1.6]. By looking at the plot it can be noticed that the classic Capacitors provide high values of specific power, but at low values of specific energy; batteries, instead, provide high specific energy at relatively low specific power. SCs perfectly fill the gap between the two systems: in particular, since different materials for electrodes and electrolytes can be chosen (and so different working principles), they occupy a big area in the Ragone plot.
Let us focus, for instance, on the comparison between a standard capacitor and a supercapacitor.

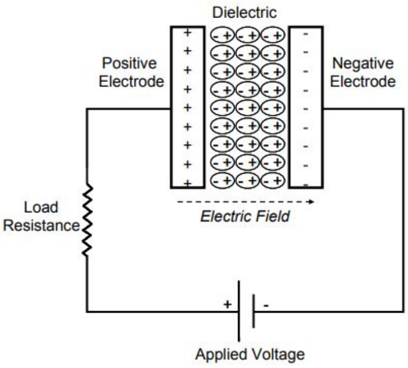

Figure 3.2: Schematic of a conventional capacitor [28]

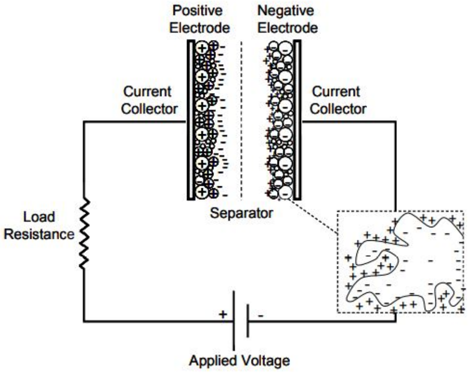

Figure 3.3: Schematic of an EDL supercapacitor [28]

In the first case, two conductive electrodes are separated by a conductive material and charges tend to accumulate at the electrodes surface when a voltage is applied [fig. 3.2]. According to this, the capacitance can be evaluated as:

$$C = \frac{Q}{V} \tag{3.1}$$

where Q is the stored charge and V is the applied potential.
To define the quality of a capacitor, we have to take into account both energy and power densities. These quantities, in fact, are those who determine the quality of a storage system. In particular, the stored energy can be computed as:

$$E = \frac{1}{2}CV^2 \tag{3.2}$$

while the maximum power corresponds to the following quantity:

$$P_{max} = \frac{V^2}{4 \times ESR} \tag{3.3}$$

We notice at first glance how the maximum power is limited by the quantity ESR. It corresponds to the equivalent series resistance, namely the overall internal resistance coming from all the components of a capacitor (current collectors, electrodes and so on) [1].

---

[1] ESR is a crucial element fro the evaluation of power density. ESR shares voltage with capacitance component during the charging step. This implies that larger ESR results in a smaller voltage for capacitance and therefore to lower energy density

Finally, for a conventional capacitor we can conclude that they are characterized by high values of power densities, but low energy densities. This means that, if compared to batteries, they store less energy, but it can be delivered very quickly. On the other hand, a supercapacitor follow the same behaviour of a standard capacitor, but with electrodes which possess an higher surface area A and thinner dielectrics (thus lower distance D between electrodes) [fig. 3.3]. Therefore, considering the following formula for the evaluation of the capacitance

$$C = \epsilon_0 \epsilon_r \frac{A}{D} \tag{3.4}$$

we can conclude that both capacitance and energy increase.
All these results are consistent with what reported on the Ragone plot, here proposed again for sake of completeness [fig. 3.4].

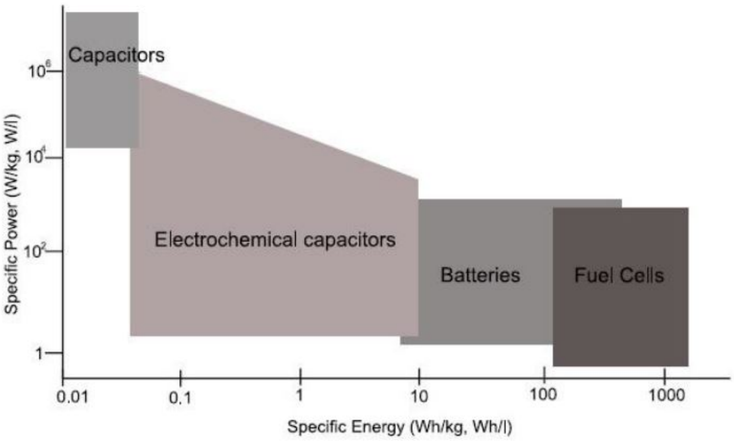

Figure 3.4: Ragone chart for energy storage devices

3.1 Working mechanism of a supercapacitor

The working mechanism of a supercapacitor has been already slightly introduced, but let us now go deeper into the topic.
Figure 3.5 shows a simple scheme of the structure of a supercapacitor.

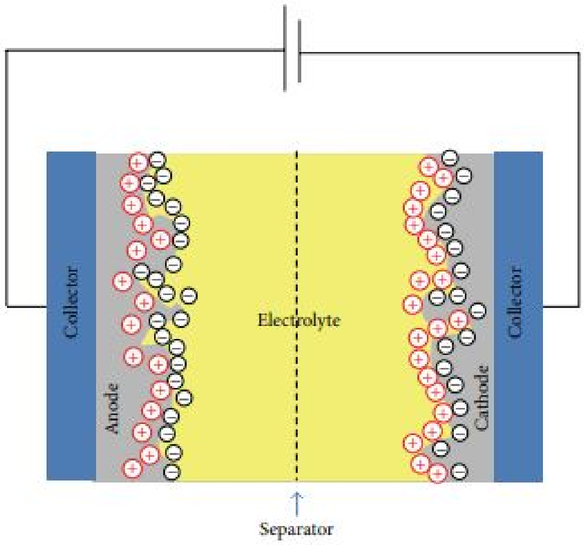

Figure 3.5: Schematic diagram of supercapacitor structure [29]

As we can observe from the above figure, a supercapcitor is composed by two electrodes usually dipped into an electrolyte (as it occurs for a battery). Charges are electrostatically accumulated at the electrode/electrolyte interface like in parallel plate capacitor. However, contrary to a conventional capacitor, no dielectric is present between the electrodes. In SCs a separator, usually made by a glass fiber, is placed. It is required in order to prevent short circuit between the electrodes that otherwise will not be isolated, but on the other hand it is permeable to ions, which are able to pass through.
In the introduction of this chapter, an important difference between conventional parallel plates capacitors and supercapacitors has been highlighted. A SC is characterized by higher surface area and lower distance between the electrodes. This is the key point of these energy storage devices. In fact, we have to think at its electrodes like a sponge, since a porous material has been deposited. In this way, ions can move inside the active material and accumulate there. These pores behaves as a uniform RC transmission line [fig. 3.6].
The equivalent circuit shows at first the distributed resistance, namely the ESR of each pore coming from the diffusion of ions from the electrolyte to the electrode.

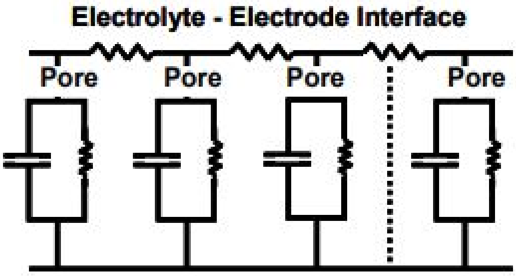

Figure 3.6: Transmission line model for a porous electrode [28]

Moreover, also distributed capacitance are present. They are an expression for the non-Faradaic double layer capacitance of each pore.
To conclude, the energy density is directly related to the surface area of the electrodes materials. A suitable choice relies on carbon nanomaterials, because of high specific surface area. Since carbon nanomaterials show excellent electrical properties, they contribute to reducing overall resistance too. Therefore, higher power density can be achieved. This last can be further increased by using electrolyte with high electrical conductivity and larger operating voltage window.

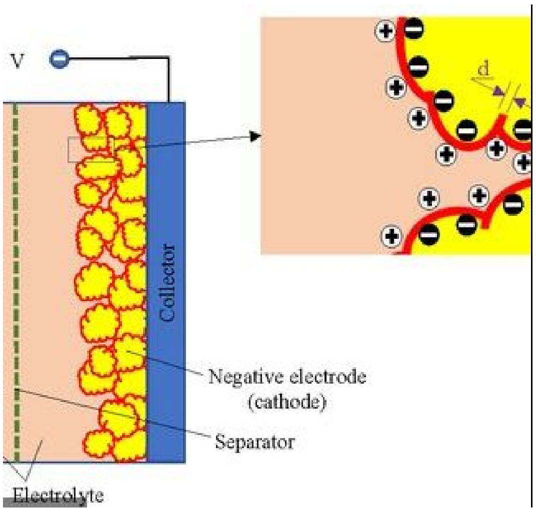

Figure 3.7: Schematic diagram of a supercapacitor revealing the EDL formed at the electrolyte-electrode interface and the separation between charged layers [30]

If conventional capacitors stores energy by moving electrons from one electrode to another, SCs store energy electrostatically through the electric double layer effect. Here, two porous plates are suspended in an electrolyte and a voltage is

applied to them. This implies an electric field into the electrolyte which causes its polarization. This causes ions to diffuse through the dielectric to the porous electrodes of opposite charges. In this way, the positive electrode attracts the negative ions dispersed into the electrolyte, while the negative electrode attracts the positive ions. An electric double layer capacitor is formed on the surface of the two plates [fig. 3.7]. As a result, distance between electrodes decreases and surface area of electrode increases.
For a supercap, the charging and discharging of the EDL capacitor is controlled purely by physical processes. As a consequence, the cycle number is high and the charging process is fast. Moreover, no chemical reaction are involved during the working of a supercapacitor, as well as no mechanical movement occurs. No pollution to the environment is produced and no noise emitted. It is a simple and small structure, ideal for energy storage device.
In conclusion, several advantages can be addressed to a SC.

1. Fast charging speed;
2. Long life cycle;
3. High energy conversion efficiency;
4. High power density;
5. Green environmental power source since non-polluting material are used;
6. High charge and discharge efficiency;
7. Easy detection and control.

3.2 Experimental section and characterization techniques

Being an electrochemical cell, the fabrication process is quite similar to the one exploited for dye-sensitized solar cells. Obviously different materials are used, but the cell is again based on an electrolyte sandwiched between two electrodes. Contrary to DSSCs, where a photoanode and a counter electrode where present, in a SC two symmetric electrodes are required.
In the following we will analyse three different supercapcitors, fabricated following the same steps, but with an active area which changes case by case.
Here we resume the experimental setup for the manufacturing of the cell.

Front and back electrode shaping:
The typical substrate for making SCs is a glass plate coated on one side with

Table 3.1: List of the SCs that will be studied in this chapter

	Active area
SC A	2x2
SC B	2x1
SC C	1x1

a Transparent and Conductive Oxide (TCO) layer, exactly as the one exploited before for the production of solar modules. This glass has to be cut with a glass knife or with a diamond cutting edge according to the desired size. Moreover, an hole has to be drilled on the surface of one of the two symmetric electrodes in such a way to allow the injection of the electrolyte in the following.

Front and back electrodes cleaning:
Same procedure exploited before. Three different cleaning steps in a sonicator working at 40 kHz: 30' in water and soap solution, 30' in Acetone and 30' in Ethanol.

Slurry preparation:
For the fabrication of the active part of our cell, we will use a carbon based slurry, made of a mixture of Activated Carbon (AC), Black Carbon (BC) and Carboxyl Methylcellulose (CMC). AC, also called activated charcoal, is a form of carbon processed to have small, low-volume pores that increase the surface area. For this reason, it is the material responsible for the higher surface area characterizing SCs. In fact, due to its high degree of microporosity, one gram of activated carbon has a surface area in excess of 3000 m^2. BC fills the voids between the particles of the main material (AC) and hence improve conductivity. CMC is a cellulose derivative with carboxymethyl groups (-CH2-COOH) bound to some of the hydroxyl groups of the glucopyranose monomers that make up the cellulose backbone. In this context, it is used as an electrode binder. Its water solubility allows for less toxic and costly processing than with non-water-soluble binders, like the traditional polyvinylidene fluoride (PVDF), therefore it is the best choice for the device that we want to produce.
In order to use as much material as possible for the production of the electrode, the limiting amount is identified as 500 mg of activated carbon, $m_{AC} = 500$ mg. Using this information, the amounts [mg] of CB and CMC are calculated as:

$$m_{tot} = m_{AC} + m_{BC} + m_{CMC} \tag{3.5}$$

See table 3.2 for the total amounts of material required for the optimized electrode.

For processing the active material, the CMC was dissolved and continuously stirred

Table 3.2: Information concerning the materials which compose the carbon based slurry used in the SC

	AC	BC	CMC
Percentage [%]	85	10	5
Weight [mg]	500	58.88	29.4

in water at a mass to volume 10:1 (29.4 mg of CMC in 2.94 ml of H_2O). Subsequently, the AC and CB were added while stirring. After the stirring was completed, the mixture was Dr. Bladed onto the electrodes with the help of a tape in order to deposit the desired area.

Slurry drying:
After the deposition of the active material, the slurry has to be dried in such a way to let evaporate the water employed during its preparation. To this aim, the electrodes are at first let dry under a chemical cap and then placed in the BUCHI setup. Here, they stay for 12 hours under vacuum condition and at a temperature of 120°C.

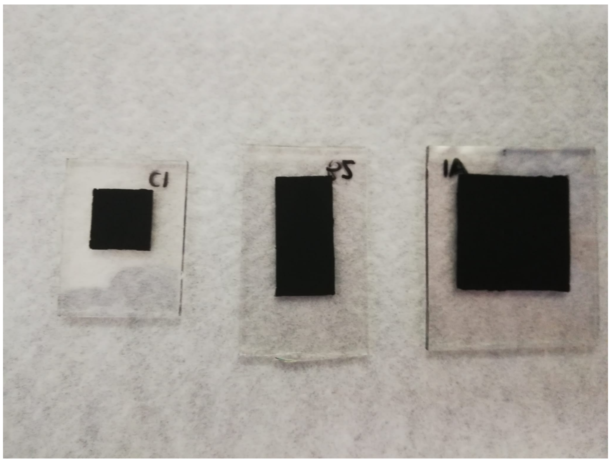

Figure 3.8: Aspect of the three different electrodes after slurry deposition and drying

Separator:
A glass fiber separator is used inside the cell in order to prevent short circuits. In particular a GF-C is used, characterized by a porous size of 1.2 µm. The "pore size" and fiber properties are sufficient to allow fair ionic mobility. Moreover,

the thickness is higher compared to polymeric separators, thus requiring a higher amount of electrolyte to let devices work properly.

Electrolyte:
The electrolyte is the ionic liquid EMIM TFSI with very high purity. 1-Ethyl-3-methylimidazolium bis(trifluoromethylsulfonyl)imide is a room temperature ionic liquid. It is as a non-aqueous solvent characterized by low vapor pressure, high thermal stability, good conductivity and a wide electrochemical window.

Cell assembly:
Once that electrodes are Dr. Bladed with the slurry and once that this last has been dried, the cell in ready to be closed. Two symmetric electrodes are put one in front of the other and a bi-adhesive tape is used to complete the sealing. Therefore, at the end we will obtain a structure similar to the one reported in figure 3.3, where the glass fiber separator is sandwiched between the carbon based electrodes.

Electrolyte injection:
At this point, the ionic liquid can be injected through the hole drilled before with the help of a syringe. Once that the chamber is filled and the separator wet by the electrolyte, the cell can be closed. In particular, a small glass cap is used.

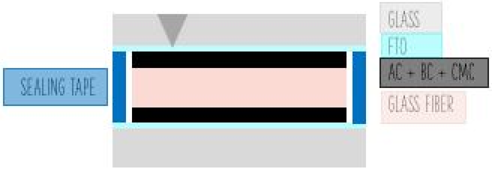

Figure 3.9: Scheme of a supercapacitor

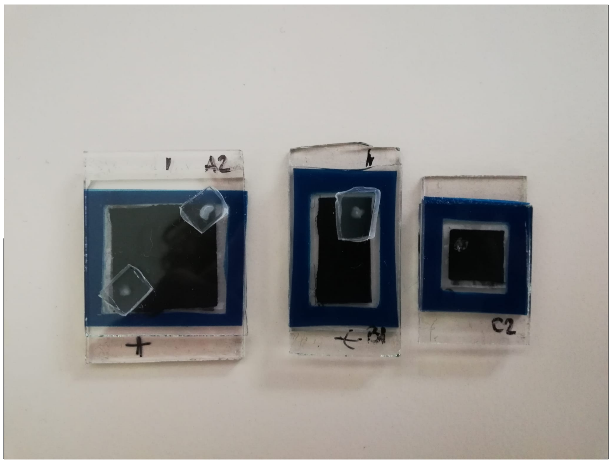

Figure 3.10: Final aspect of the fabricated supercapacitors

Let us now introduce briefly the different techniques used to investigate the behaviour of the three devices.
The first approach that we are going to describe is the *charge-discharge Galvanostatic (CDG)* method. It consists in charging and discharging the supercapacitor

between two defined voltage values by applying a constant current; often, this process is repeated for multiple cycles. Ideally the curve described by the voltage response is linear, with two opposite slopes corresponding to charge and discharge processes. CDG profile is used, for instance, to evaluate the capacitive response of a device by exploiting the slopes of the voltage response ($C = \frac{i}{dV/dt}$). Since we are dealing with real devices with losses, it is possible to note non-ideal behaviours on the potential-time plot [fig. 3.11].

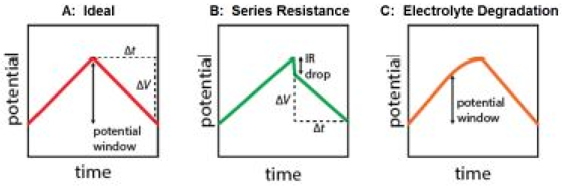

Figure 3.11: Non-ideal effects in CDG measurement

Considering the effect of resistive elements, it is possible to appreciate a voltage drop (iR-drop) when the device switches from charge to discharge process. iR-drop occurs due to the ESR offered by the supercapacitor. Some of the potential is used up to overcome this resistance while the rest of the potential is used to charge the supercapacitor. The circuit can be imagined as a capacitor and a resistor joined in series. The voltage drop due to the series resistance gives the iR drop. Moreover, the electrolyte may degrade, causing inflection points on the trend and a no longer clear transition between charge and discharge.

Another possible electrochemical technique for characterizing the device is the *Cyclic Voltammetry (CV)*. Usually this method is used in a three electrode configuration, consisting in a counter electrode, a reference electrode and a working electrode: the voltage applied to the electrode immersed in the electrolyte solution is used as the control quantity to study the response of the system. In CV measurements, the potential of the working electrode is analyzed with respect to a reference electrode which is maintained at a constant voltage. The potential difference between the working electrode and the reference electrode is swept in time between an upper and a lower limits, thus allowing to have multiple ramps and therefore different cycles [fig. 3.12].

Simultaneously a current flows between the working electrode and the counter electrode, which is recorded as a function of the potential. The current is dependent on the potential scan rate and it is possible to obtain it by the slope of the potential-time plot.

In a capacitive electrochemical cell, by letting the voltage sweep linearly between two potential boundaries, the voltammogram (current-potential trend) follows the

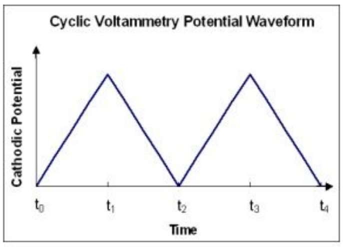

Figure 4: example of a control signal for CV

Figure 3.12: example of a control signal for CV

general trend shown in figure 3.13.

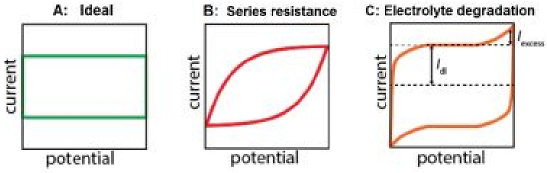

Figure 3.13: Voltammogram for CV

In particular, if the voltage is swept linearly over time and by considering the equation

$$i(t) = C\frac{dv}{dt}, \tag{3.6}$$

then the ideal Voltammogram has a rectangular shape with constant currents (positive current when the voltage increases and negative when the voltage decreases). As in the CDG case, there will always be a deviation from the ideal behaviour because of the series resistance in the system (contacts, terminals, diffusion of ions in the electrolyte) and of the electrolyte degradation.
The last method that we will use is the electrochemical impedance spectroscopy (EIS). In this approach a superposition of a sinusoidal signal with a small amplitude over a DC voltage is used to perturb the system. The system response is an AC current. Usually the resulting impedance is represented by a real part and a complex part.

$$Z(\omega) = Z'(\omega) + Z"(\omega) \tag{3.7}$$

It is possible to plot the computed impedance in two different ways. The EIS data can be represented in the complex plane where on the x-axis there is the real part of the impedance Z', while on the y-axes there is the complex part Z"; this representation is called Nyquist plot.

The other way consists in to plot the impedance modulus and the phase versus frequency; these graphs are known as Bode plots.
It is possible to use the EIS data to create a model that contains Equivalent Electrical Circuit (EEC) elements where every element (capacitor, inductor, resistor) describes a physical process in the system.
Three general circuits which describe the system are reported in the following figure with the respective Nyquist plots.

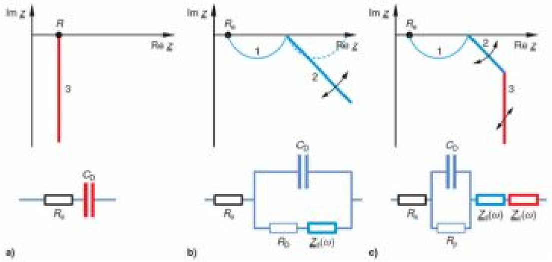

Figure 3.14: General equivalent circuits: (a) ideal behaviour, (b) diffusion in mesopores, (c) diffusion impedance in macro pores

3.3 Results and data analysis

Before proceeding with the characterization of the device, it is interesting to investigate the amount of carbon slurry which have been deposited on each electrode. In fact, according to literature, usually the supercapacitors are characterized in terms of gravimetric quantities.

Table 3.3: Weights of deposited slurry for each electrode

	Before the deposition	After the deposition
A1	4.1618 mg	4.1695 mg
A2	4.17358 mg	4.1840 mg
B1	3.0050 mg	3.0103 mg
B2	3.0514 mg	3.0561 mg
C1	2.1093 mg	2.1133 mg
C2	2.2157 mg	2.2197 mg

According to table 3.3, we can extrapolate the effective amount of slurry which has been Dr. Bladed for each supercapacitor.

Table 3.4: Relative amount of active material for each device

	weight of active material [mg]	weight of active material per unit area [mg/cm^2]
SC A	18.44	4.61
SC B	10	5
SC C	8	8

At this point, we are ready to characterize the devices. Let us at first perform a cyclic voltammetry on each of the supercapacitor. The measurement implies a variation of the applied potential at the working electrode for both forward and reverse directions at a fixed scan rate (in this case, dE/dt = 5mV/s) while observing the current. 8 cycles are implemented, in such a way to observe the stability of the SC. The measurements are performed on two potential windows: 0V-1V and 0V-2V.

From the graphs it is possible to compute the respective capacitance inverting equation 3.6, from which we obtain:

$$C = \frac{\int_0^t i(t)dt}{dV} \tag{3.8}$$

It is now interesting to look at the shapes of the cyclic voltammetry curves obtained.

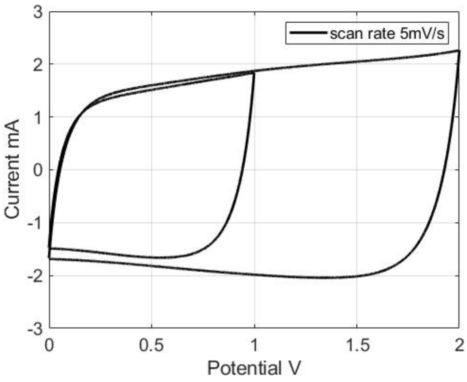

Figure 3.15: Last CV cycle for device A

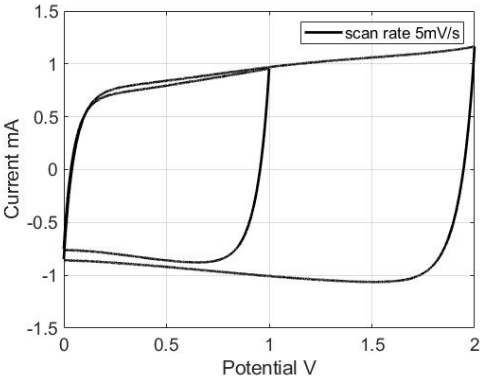

Figure 3.16: Last CV cycle for device B

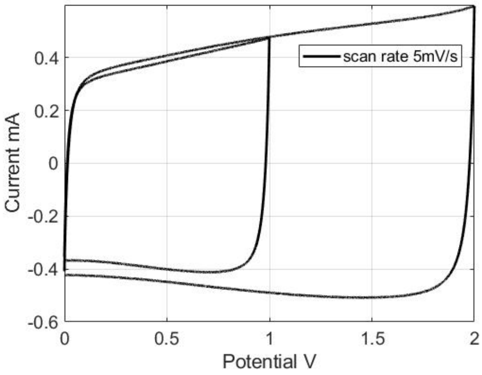

Figure 3.17: Last CV cycle for device C

Table 3.5: Capacitances for devices A, B and C get from CV measurement

Device	Window [V]	Capacitance [mF]	Capacitance [mF/g]	Capacitance [mF/cm^2]
A	0-1	283	15.34	70.75
A	0-2	353	19.14	88.25
B	0-1	152	15.2	76
B	0-2	185	18.5	92.5
C	0-1	75	9.375	75
C	0-2	92	11.5	92

As mentioned before, an ideal defects less device should have a perfectly rectangular CV, since it ideally behaves like a electric double layer capacitor. Of course, our devices do not work in an ideally way and therefore the shape of the CV curves is not a perfect rectangular. The reason for the deviation from an ideal shape can be addressed to the series resistance, responsible for capacitance losses (smaller CV area means smaller capacitance). In fact, just the employment of a glass electrode gives a huge contribution to the resistance, since FTO has a quite high value of R_s; if we had used, for instance, a metal electrode, this resistance would has been lower. Resistances' contributions can be highlighted also looking at the results obtained with an electrochemical impedance spectroscopy analysis [fig. 3.18].

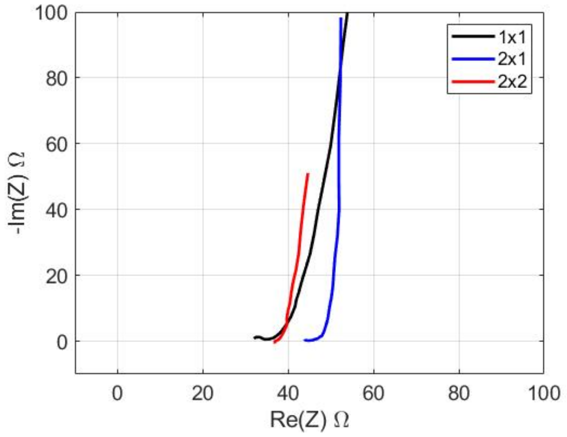

Figure 3.18: EIS for the devices A, B and C

This last picture allows us to evaluate the amount of the series resistance for each device.

Table 3.6: Series resistances for devices A, B and C

Device	R_s [Ω]
A	36.94
B	43.81
C	32.25

Table 3.6 shows values of series resistance which are quite high for the kind of the devices that we are testing. This derives from the fact that we are using a glass collector, instead of a metal one, as mentioned before. Moreover, this implies that our supercapacitors have a quite high resistive behaviour, even if a good level of stability can be observed from the cyclic voltammetry. However, figure 3.18 is not so satisfactory for what concerns device C. By looking at the curve plotted after the EIS measurement we notice that it is not in line with devices A and B, therefore probably it is not working in a proper way, maybe because of some error

during the fabrication process.
Looking again at the cyclic voltammetries, other information can be achieved. In particular, we do not observe peaks at the corner of the CV, that usually are a consequence of the electrolyte degradation. They would correspond to irreversible processes that could happen inside the electrolyte, but fortunately it seems that this is not our case. Here we have used a ionic liquid as electrolyte, but if on the other hand we had used an aqueous electrolyte, for instance, we would have observed some peaks in correspondence of 0.8 V, where water electrolysis starts.
One last remark concerning the CV is that they are quite stable in both potential windows. This means that our devices are able to work in a stable way in both ranges of voltage. This is a great result especially for the window 0V-2V, since we will integrate this supercapacitor with a solar module of $V_{oc} \sim 2V$.

Another analysis can be implemented on the devices in order to have an evaluation of their capacitance: charge-discharge galvanostatic. In particular, we perform the galvanostatic analysis at a fixed current of 1 mA.
In a CDG, for higher currents the charge process behaves in a different way with respect to the case of low ones. In fact, when a small current is applied, the charge cycle is very slow and the achieved capacitance will be higher. This is due to the fact that our electrode is constituted by a porous material; when the charge is slow, ions have the time to slip into the porous structure and accumulate there in such a way to charge the device. On the other hand, when the current is higher, the charge cycle is faster and ions do not have the time to slide in a proper way into the porous electrode, therefore the capacitance will be smaller since less ions accumulate.
However, having low currents not only implies higher capacitance but also the possibility that more irreversible reactions occur. In fact, since the charge cycle is slow, the device will be charged over the threshold potential for electrolyte degradation for a longer time, with the risk of damage for the device. On the other hand, a fast charge means a small period of time over the threshold voltage for these irreversible reactions and therefore a lower risk of degradation.

By looking at figure 3.19, we observe at first glance the presence of an iR drop. We have already mentioned the meaning of this drop, namely it depends on the resistance offered by the supercapacitor. It is a quantity which takes into account the ESR of the device, giving a measure of its resistivity.
Moreover, by the discharge profile, we can compute the capacitance for every device as:

$$C = \frac{i}{dV/dT} \tag{3.9}$$

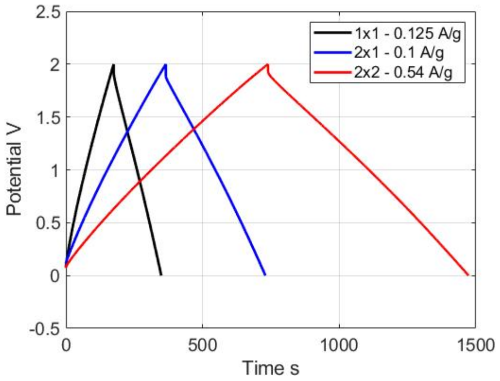

Figure 3.19: CDG for devices A, B and C at constant current of 1 mA

Therefore we get:

Table 3.7: Capacitances for devices A, B and C from CDG measurement

Device	Capacitance [mF]	Capacitance [mF/g]	Capacitance $[mF/cm^2]$
A	382.2	20.7	95.55
B	193.7	19.37	96.85
C	91.1	11.38	91.1

In addition to this, other CDG measurement at different constant currents has been performed. However, we have noticed that our devices do not bear higher values of current since a too much resistive behaviour occurs.

To conclude the analysis, one last parameter of interest can be computed. It concerns the coulombic efficiency, namely the ratio between the charge in the discharge cycle and the charge in the charge cycle:

$$\eta = \frac{Q_{discharge}}{Q_{charge}} = \frac{i \times t_{discharge}}{i \times t_{charge}} \tag{3.10}$$

From figure 3.19, the following data are achieved [tab. 3.8].

Table 3.8: Coulombic efficiencies for device A, B and C

Device	Q_{charge} [C]	$Q_{discharge}$ [C]	Coulombic efficiency [%]
A	0.739	0.733	99.15
B	0.366	0.364	99.59
C	0.175	0.174	99.36

At this point, by comparing tables 3.5, 3.7 and 3.8, we can look at the achieved capacitance and coulombic efficiency for each device in order to choose which is the best one for our final integrated energy harvesting and storage module. In particular, observing the data, we can notice that the best performances are achieved for devices B, namely the one with dimensions 2x1. In fact, it is the one with higher capacitance values per unit of mass and area.

Chapter 4

Integrated HS device

The main issue of standard EES systems is that they require an external power source and continuous maintenance in order to work. This can be very challenging, therefore the need to develop a self-powered device with multi-functional properties (i.e. energy harvesting and storage components) becomes necessary.
Zhong et al. reported different types of integration for multi-functionality [31]. One is called joint combination and it is based on different devices, each one with its own function, which are connected one with respect to the others. In particular this combination can occur in two ways: integrated combination and discontinuous connection. The second kind of integration concerns the realization of one unit with multiple purpose, namely one single component which process different activities. Here in the following we will take into account the joint combination based on integration, in which several components are intrinsically connected one to the other without the need of any external wire.

4.1 Experimental section

In order to fabricate an energy harvesting and storage device, we follow the same procedures already exploited in previous sections. In particular, our system is made of a supercapacitor with dimensions 2x1 (choice made as result from previous analysis on different EDLCs) and of a dye-sensitized solar module composed by three cells [fig. 4.1].

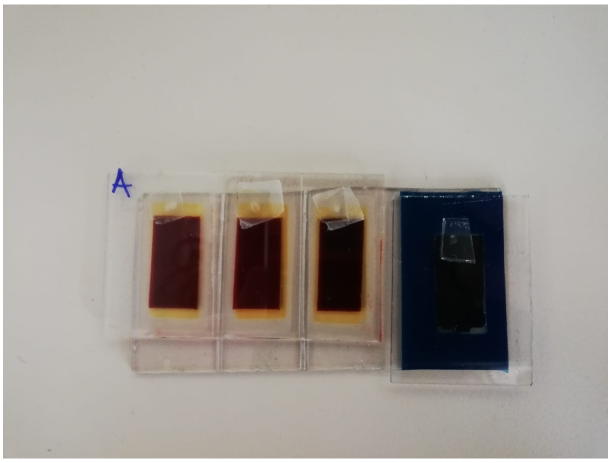

Figure 4.1: Picture of the integrated energy harvesting and storage module fabricated in our laboratory

In particular, we aim to fabricate a 3-electrode HS device, in which two different systems share an electrode. Since we will produce, in a second moment, a bifacial-tandem HS device, we establish that the counter electrode of the DSSM will be the electrode in common between the two devices. Therefore, on a unique glass electrode, we will have three Pt cathodes and one carbon-based electrode for the supercapacitor. Then, other two separated glass electrodes will be prepared, in such a way to fabricate the photoanode for the solar module and the symmetric electrode for the EDLC.

Front and back electrodes shaping:
We have at first to prepare the glassy material for the electrodes. As before, we use TCO16-15 provided from Solaronix, namely a glassy layer with one side covered by FTO, a thickness of 16 mm and a sheet resistance of 15 Ω square. The desired shapes are obtained with a glass knife and three different pieces are achieved. A big one (4cmx8cm) which will host Pt counter electrodes and back electrode of the supercapacitor. A smaller one (4cmx6cm) for the fabrication of the photoanodes. An even smaller (3cmx4cm) for the front electrode of the supercapacitor. Moreover,

the electrodes of the DSSM have to be engraved with a diamond cutter in order to allow the fabrication of a Z-module and therefore a proper path for the current. Finally, holes have to be drilled on the surface of the photoanode, in correspondence of the three cells, in such a way to be able to vcuum fill the chamber with the electrolyte.

Front and back electrodes cleaning:
Same cleaning process exploited before. 30’ in water soap, 30’ in Acetone and 30’ in Ethanol. Then the solvent are let evaporate on a hot press held at 100 ° C.

Photoanode:
Three different photoanodes are fabricated, each of them with an active area of 2 cm^2 (dimensions are 2cmx1cm). In order to have the possibility to create a bifacial-tandem device, they have to be transparent. To this aim, transparent TiO_2 paste T/SP provided by Solaronix is used. It is Dr. Bladed on the conductive side of the glass electrode and then let sinter in a muffle at 450 ° C. When the cycle finishes, photoanodes are dipped into the N719 dye and let soaking for almost one day.

Counter electrode:
A very thin Platinum layer is deposited through sputtering. To guarantee a good level of transparency, the sputtering time is reduced to 10s. Also in this case, three counter electrodes (2cmx1cm) are sputtered, aligned with the photoanodes previously fabricated.

Contacting the cells:
In order to electrically connect the cells which are separated because of the incisions done before, a conductive medium has to be deposited in order to allow the current to flow all along the solar module. We use again Silver conductive RS 186-3600, which is Dr. Bladed onto the counter electrode closed to the incisions in such a way to not loose area.

DSSM assembly and electrolyte injection:
Once that both photoanodes and counter electrodes are ready, the module can be sealed. At first, we prepare three gaskets from a thermoplastic material. Each of them is located around each photoanode, then the counter electrode is leaned on it and the whole system is carried on a hot press. Here, high temperature melts the thermoplastic tape and the two electrodes attach each others. At this point, the chamber can be vacuum filled with the Iodine-based electrolyte. A syringe is brought in proximity of the hole previously drilled such that the electrolyte can flow into the chamber. Once that it is full, it is closed with a glass cap put on top

of the hole. In this way, the fabrication of the DSSM is completed.

Supercapacitor:
For the supercapacitor, one carbon based electrode is fabricated on the same glass of the counter electrodes, while the other on a separated layer. The same carbon slurry exploited before is used, again with 85 % of Activated Carbon, 10 % of Black Carbon and 5 % of CMC. Once that the slurry has been deposited (Dr. Blade technique) and dried (12 hours cycle in the BUCHI), it can be sealed. At first, a fiber glass separator is put between the active electrodes in order to prevent short circuit, and then the cell is closed with the help of a tape. Finally, ionic liquid EMIM TFSI is injected into the chamber through a hole previously drilled and then close with a glass cap.

What shown up to now, was the process for the fabrication of an integrated energy harvesting and storage device. However, our aim is to create a bifacial-tandem energy HS device, therefore another solar module is required. To this aim, we will use again the module B [IV characteristic in fig. 2.23] already presented in previous chapters. In this way, we can put in contact both module counter electrode and integrated device [fig. 4.3] counter electrode, such to exploit bifacial and tandem properties of our final device.

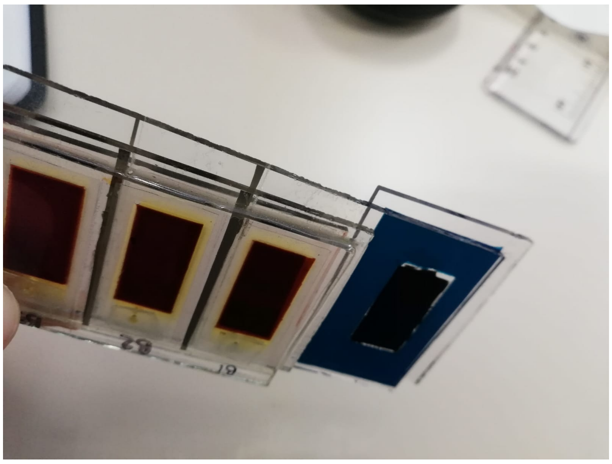

Figure 4.2: Side view of bifacial-tandem integrated HS device

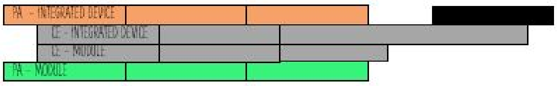

Figure 4.3: Scheme of bifacial-tandem integrated HS device

4.2 Results and data analysis

In this section, we will report the results obtained by the characterization of the bifacial-tandem integrated energy harvesting and storage module. In particular, we will characterize at first the supercapacitor belonging to the integrated module alone, namely without the influence of the DSSM. Then we will test the performances of the dye-sensitized solar module. Finally, the complete integrated device will be characterized, both in standard and in bifacial-tandem configurations. To better appreciate the performances of our integrated HS device, the combined efficiency of both DSSM and SC will be evaluated.

4.2.1 The supercapacitor

For what concerns the supercapacitor, we perform a CV, an EIS measurement and a CDG at the end.
Exactly as before, the cyclic voltammetry is performed for two different potential windows: 0V-1V and 0V-2V. Once again, this leads us to understand if the device is stable in both operating regions, in order to find out if the integration with a module that works at, more or less, 2V is possible. As in the previous case, the test is carried on at a unique scan rate: dE/dt = 5mV/s.
By looking at the shapes of the CV curves reported in figure 4.4, we observe a quite good behaviour. The illustrated cycle is the last one, therefore we can assume that the device is sufficiently stable. Actually, the shapes deviate from the ideal rectangle, but are not so resistive. In fact, they almost fill the expected area with no peaks present at corners, meaning that any irreversible reactions in the electrolyte is damaging the performance of the device.
Thanks to CV measurement, and exploiting equation 3.8, it is possible to measure the capacitance in both potential windows.

Table 4.1: Capacitance from CV measurement

Window [V]	Capacitance [mF]	Capacitance [mF/cm^2]
0-1	156	78
0-2	189	94.5

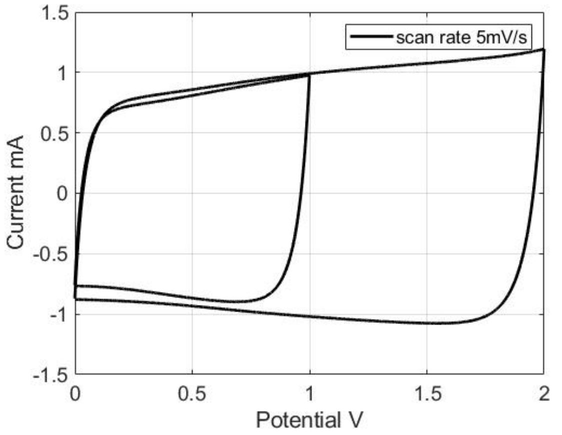

Figure 4.4: Last cycle for CV measurement

Let us remember that here we are characterizing a supercapacitor with dimension 2x1 (area of 2 cm^2). The obtained capacitance are in fact quite similar to the ones obtained for device B in table 3.5 [1].
At this point, we can proceed as in the previous chapter and focusing on the resistive behaviour of the device by performing an electrochemical impedance spectroscopy [fig. 4.5]. In this way, we can achieve a measure of the ESR of the supercapacitor.

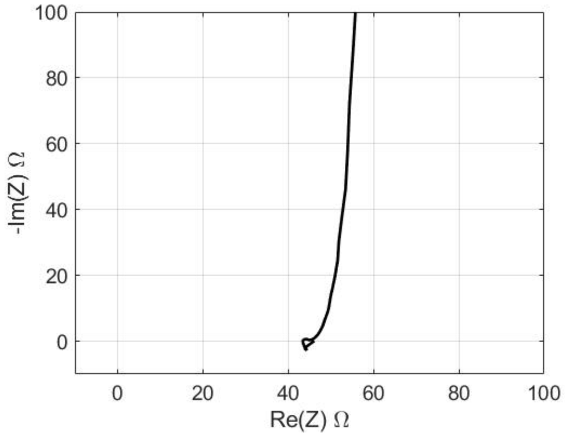

Figure 4.5: EIS

---

[1] Actually, the capacitance and the capacitance per unit area are not exactly the same, because of the fabrication process. Even if the steps for their fabrication are the same, some differences may arise.

The obtained series resistance from EIS measurement is 43 Ω, almost in accordance with the cases analysed before. In fact, it is quite high even in this occasion, but we can justify this amount by considering the fact that we are using a glass electrode, intrinsically provided by a pretty high series resistance.
To conclude, a CDG at a fixed current of 1 mA is performed.

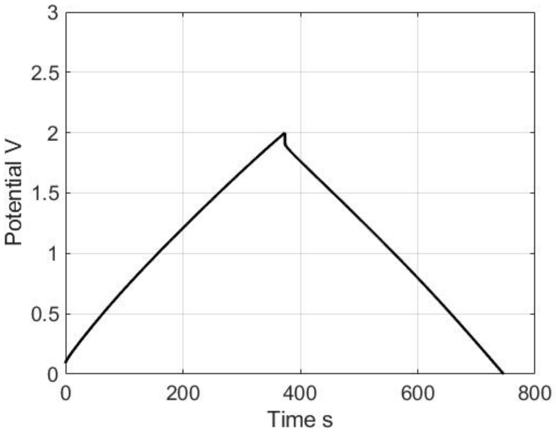

Figure 4.6: Last cycle for CDG at 1mA

Here we observe again the presence of the iR drop, consequence of the ESR of the device. On the other hand, both charge and discharge profile are quite linear, meaning that no electrolyte degradation is occurring.
At this point, from equation 3.9, the capacitance coming from the discharge profile can be computed: 195.4 mF (97.5 mF/cm^2). As well as before, we conclude the analysis with the evaluation of the coulombic efficiency [eq. 3.10].

Table 4.2: Coulombic efficiency

Q_{charge} [C]	$Q_{discharge}$ [C]	Coulombic efficiency [%]
0.374	0.373	99.6

4.2.2 The dye-sensitized solar module

Let us now take into account the bifacial-tandem DSSM. Here we characterize the combination between the module B described in chapter 2 and the module of the integrated device just fabricated and presented in this chapter. As usual, an IV measurement is performed and the most relevant parameters are extracted from the analysis.

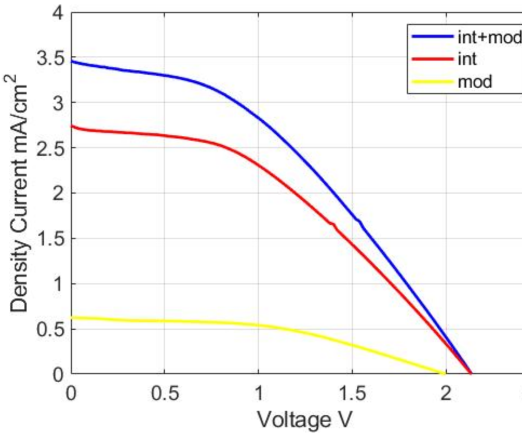

Figure 4.7: IV characteristic for the bifacial-tandem integrated energy harvesting module: integrated module on the top, DSSM on the bottom

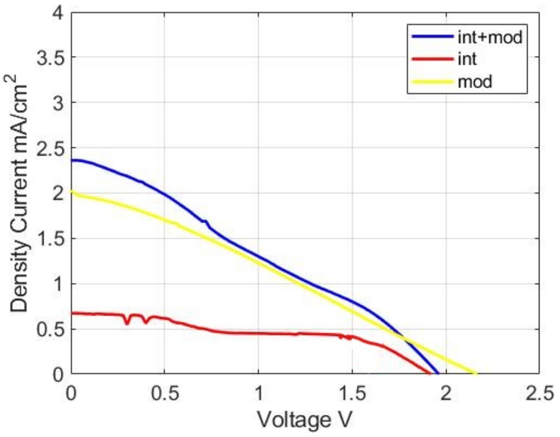

Figure 4.8: IV characteristic for the bifacial-tandem integrated energy harvesting module: integrated module on the bottom, DSSM on the top

Figures 4.7 and 4.8 show the IV curved respectively for the case in which the integrated device is directly illuminated by the incoming radiation, while the module is beneath it and viceversa. At first glance, we can observe that the two graphs are not so similar as it occurs when we compared module A and module B [fig. 2.22 and 2.23]. To better appreciate this discrepancy, let us list the parameters characterizing the performances of the device.
By looking at efficiencies and current density values in table 4.3 and 4.4 we notice some differences. It seems that bifaciality properties are not longer valid, since the bifacial device behaves better when illumination is provided towards the integrated module rather than towards module B. However, this can be simply justified by considering the time in which both devices were fabricated. View that, module B has been produced almost a week before the integrated device, we can conclude that module's performances have been deteriorated.
Despite the poor ability of the module, we can still observe some advantages related to the bifacial-tandem configuration. Looking at table 4.3 we can notice that both short circuit current density and efficiency reach higher values with respect to a

Table 4.3: Characterization parameters related to figure 4.7

	INT+MOD	INT	MOD
$V_{oc}[V]$	2.14	2.14	1.99
$J_{sc}\ [mA/cm^2]$	3.45	2.74	0.62
FF	0.40	0.41	0.46
η [%]	3.27	2.66	0.64

Table 4.4: Characterization parameters related to figure 4.8

	MOD+INT	MOD	INT
$V_{oc}[V]$	1.96	2.17	1.91
$J_{sc}\ [mA/cm^2]$	2.36	2.02	0.67
FF	0.28	0.28	0.48
η [%]	1.45	1.37	0.69

non bifacial-tandem configuration. In fact, as already said, view that the incoming radiation which is not absorbed by the first module can be collected by the second one, the photo-generated current will be higher and so does the efficiency. Moreover, we have also tested the performances of the single modules while connected in a bifacial-tandem configuration. This means that we have at first contact only the integrated module and then the underlying module B. For this last, lower values of density current are achieved, because this module is actually covered by the other one which is directly faces the illumination source. Furthermore, looking at both density currents, we can notice that their sum is almost equal to the photo-generated current of the bifacial-tandem module. The same behaviour can be observed by considering the efficiencies too. Therefore, also in this case we can say that the parallel connection is working and that the overall performances of the device have been boosted. The same results are achieved for the other configuration, where the module B is directly illuminated by the incoming radiation and the integrated module is screened.

4.2.3 The bifacial-tandem integrated energy harvesting and storage module

At this point, after having characterized both DSSM and supercapacitor, we can analyse how these device work when they are in an integrated configuration.
The main tool that we have for this kind of characterization is the photo-charge and discharge measurement. It resembles a standard charge discharge galvanostatic measurement, but with the important difference that the applied current for the charge cycle is not fixed. In fact, the charging current arises from the DSSM which is under illumination and therefore it is generating a photo-current.
In particular, the HS integrated device is put inside the sun simulator (in this case we consider an incoming intensity of 0.9 sun). Both DSSM electrodes and EDLC electrodes are contacted by a Keithley sourcemeter and, once that light is turned on, the multimeter terminals measure the photo-changing EDLC voltage.
During the charge phase, we expect that supercapacitor voltage rises up to 2V, approaching the V_{oc} of the PV part. For the discharge cycle, the solar module is electrically disconnected and a negative current of 1 mA is applied to let the storage device completely discharge. We choose this value in order to stay in the same order of magnitude range of the photo-charging current. In fact, from previous analysis on PV devices, we have seen that a maximum current of about 3mA can be generated. In this way, a similar step time with respect to the photo-charge can be granted.

Let us characterize the integrated energy HS device with a photo-charge discharge measurement.

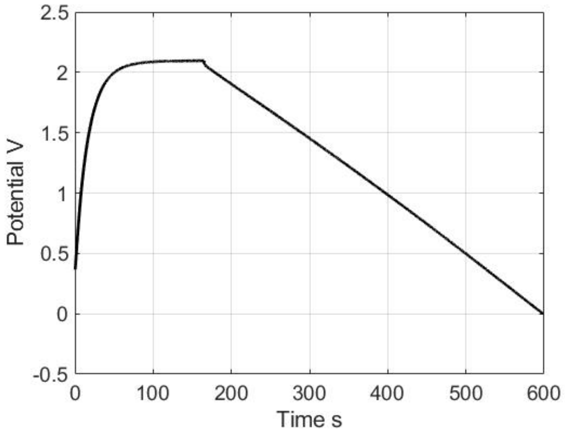

Figure 4.9: Photocharge and discharge for the integrated module

Figure 4.9 shows photo-charge and subsequent discharge curves for one constant current of 1mA.

Looking at the charge profile, we observe a slightly linear increase of the voltage up to reach a plateau around 2V. In particular, the maximum voltage that can be achieved by the charge cycle is 2.095 V, value which is very close to the V_{oc} of DSSM (2.14 V). More in particular, a deviation from linearity can be observe already around 1V, but this is perfectly in accordance with the IV profile [fig. 4.7, red line, the one related to the integrated device], since, up to 1V, no evident decrease are observed in photo-generated current with respect to the maximum current point (short circuit current). Over this threshold, the slope is rapidly changing until the plateau is reached after 182 s. Therefore, the charging time for the integrated HS device is of nearly 3 minutes.

On the other hand, by looking at the discharge profile, we notice a very linear trend from which we can evaluate the capacitance of the supercapacitor integrated in our device. According to equation 3.9 we get a capacitance of 104.9 mF/cm^2, quite similar to the one obtained before with CDG measurement (97.5 mF/cm^2).

Let us now introduce an important parameter that allows us to determine the quality of our device: the efficiency. If for both dye-sensitized solar cells and supercapacitor the evaluation of the efficiency is quite simple because of the huge amount of related information in literature, for what concerns a HS device things are more tricky. In fact, as mentioned many times, for a PV device the efficiency can be easily computed as the ratio between the maximum power point achieved by the IV measurement and the radiation power incident on the device, while for a supercapacitor the coulombic efficiency is basically the ratio between the charge in the discharge cycle and the charge in the charge one.

For what concerns an integrated HS device we have to take into account that, as previously outlined, at a certain point, a plateau is reached. On one side this is useful since ions become able to arrange into the porous structure, but on the other side the energy coming from the impinging radiation is wasted since the voltage of the supercapacitor is not increasing anymore.

Keeping in mind all these considerations, we can proceed computing the overall efficiency of the integrated device. According to the majority of papers, the most used method in literature relies on the OPECSE. This word stands for overall photon-to-electron conversion and storage efficiency and can be computed as follows [32].

$$OPECSE = \frac{\frac{1}{2}CV^2}{GtS} \tag{4.1}$$

where C is the capacitance of the supercapacitor computed by the discharge profile of the photo-charge measurement (209.8 mF), V is the maximum voltage achieved

during photo-charge (in correspondence to the plateau), G is the electromagnetic power density impinging onto the DSSM (90 mW/cm^2), t is the photo-charging time and S is the active area of the solar module.
However, it is more interesting to evaluate the OPECSE in terms of EDLC voltage and charging times in order to see which levels of overall efficiencies can be achieved according to the voltage to which the EDLC is charged.

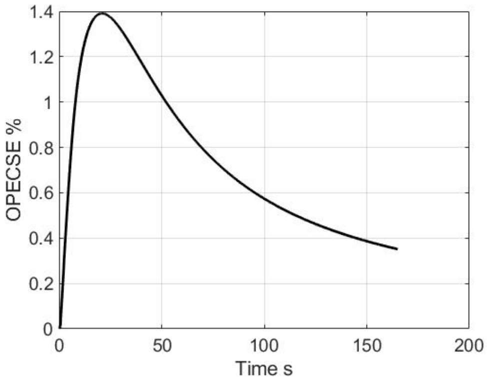

Figure 4.10: OPECSE plotted as a function of the charging time

Figure 4.10 shows how the OPECSE changes all along the charging cycle. At first, we observe a pretty linear trend between voltage and time. Then, we can notice at first glance that the maximum is not achieved for the highest value of voltage at which the supercapacitor can be charged. Actually, we reach the best OPECSE of 1.39 % at 1.58 V after 20 s. This is still a good result if we consider that practical applications (IoT) usually require units of Volt in order to be correctly supplied. After the peak, the OPECSE starts to decrease since the supercapacitor voltage is approaching the open circuit voltage of the solar module, thus reducing the amount of energy that can be stored in the EDLC.
To further prove this result let us consider the OPECSE in terms of EDLC voltage.

From figure 4.14 we can again demonstrate that the maximum OPECSE is reached at 1.58 V, exactly as shown in the previous graph.

At this point, we would like to perform the same analysis for a bifacial-tandem integrated energy. To this aim, let us characterize the configuration in which we have the integrated HS device placed on top of DSSM B.
From figure 4.12 we can observe how photo-charge behaves for this configuration. The shape of the achieved curve is quite similar to the one obtained before. We observe at first a linear trend of the potential with respect to the time, up to the plateau. It is interesting to notice that in this case the potential at which the SC is

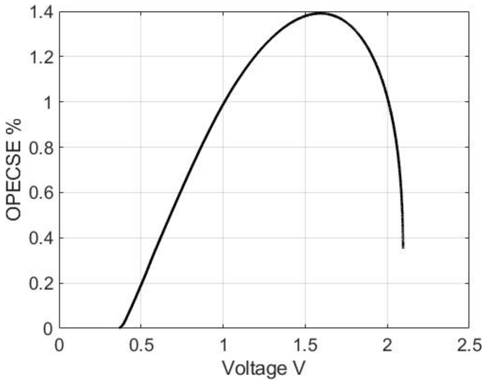

Figure 4.11: OPECSE plotted as a function of the EDLC Voltage

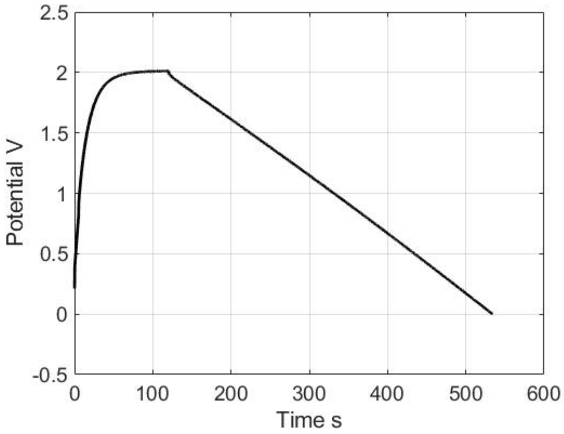

Figure 4.12: Photocharge and discharge for the integrated module in bifacial-tandem configuration: integrated module on the top, DSSM on the bottom

charged saturates is quite similar with respect to before case (2.011 V wrt 2.095 V). This can be justified by the fact that the two solar modules show an open circuit voltage which is pretty the same, as we have noticed during the characterization of the harvesting part in this chapter.
At this point, from the photo-charge analysis, we can evaluate some quantities of interest listed in the following table.

From table 4.5 we can at first notice that the capacitance values are quite similar to the ones achieved before. This is justified by the fact that the capacitor is the same, since what is changing in this configuration concerns only the harvesting section.
Moreover, a more interesting focus concerns the charging time. Here the SC is

Table 4.5: Parameters extracted from photo-charge measurement for bifacial-tandem integrated HS device

Capacitance [mF]	Capacitance [mF/cm^2]	Charging time [s]
208.5	104.25	120

charged in 120s. If we compare this result with the one previous obtained for the integrated HS device we notice that it is quite lower. This is perfectly in accordance with what was expected, since we have to consider that the photo-generated current density by the bifacial module is higher. Therefore, the charge cycle will be driven by an higher current and as a consequence the EDLC will be charged sooner.
Finally, the evaluation of the combined efficiency (OPECSE) can be performed.

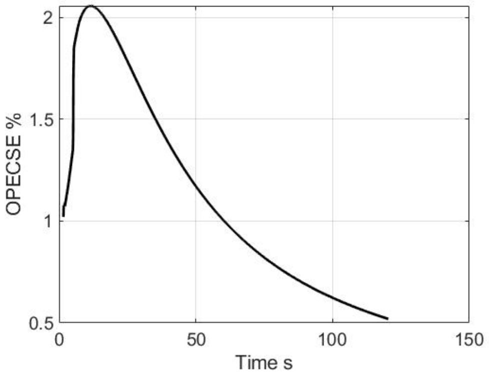

Figure 4.13: OPECSE plotted as a function of the charging time

Figure 4.13 shows how the OPECSE changes all along the charging cycle. Unfortunately, we immediately observed that the trend of the curve is not coherent with the one discovered before, at least for what concerns the first part. This can be explained by the way in which contacts occur. Some noises are present in this first section, probably due to the way in which DSSMs were contacted.
However, what with are really interested in, is not affected by this kind of problems. In fact, we can still observe a pretty linear trend between voltage and time, as did before. Then, we can notice once again that the maximum value for the OPECSE is not achieved for the highest value of voltage at which the supercapacitor can be charged. Actually, we reach the best OPECSE of 2.06 % at 1.13 V after 12 s.
We can easily observe the advantages of a bifacial-tandem configuration. In fact, having a double layer of photo-sensitive elements allows higher photo-generated

currents, therefore a faster charge for the SC and higher values of combined efficiency.
To further prove this result let us consider the OPECSE in terms of EDLC voltage.

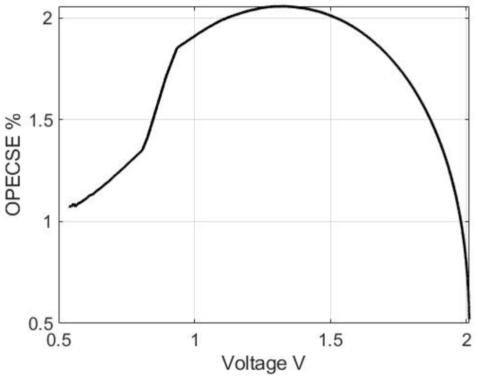

Figure 4.14: OPECSE plotted as a function of the EDLC Voltage

From figure 4.14 we can again demonstrate that the maximum OPECSE is reached at 1.13 V, exactly as shown in the previous graph. Unfortunately, as for figure 4.13 some discrepancy is observed at the beginning of the charging cycle. Even in this case, it can be addressed to some noises coming from the contact, since we have to take into account that two different contacts have to be placed: one for the integrated module and one for the underlying one. Therefore, disorders may arise.

Chapter 5

Conclusions

Energy harvesting and storage integrated devices are acquiring more and more importance in nowadays technological framework. Since the growing relevance of smart objects belonging to the IoT world, researches have to go on in such a way to avoid devices which have to be charged daily or batteries that have to be replaced constantly. New alternatives have to be found in order to harvest energy in a way suitable with the Internet of Things world. An integrated HS device like the one studied during the course of this thesis is one of them.

In particular, in this work, the integration between a dye-sensitized solar module and a supercapacitor has been implemented. At first, we focused on the characterization of the harvesting part of the device and then the storage one was taken into account. In this thesis, DSSCs have been further analysed, focusing on the fabrication of both standard and innovative technologies. In particular, the goal was to create a bifacial-tandem dye-sensitized solar module in order to achieve a device which exploits both bifacial and tandem properties. In this way, we have observed at first the importance to have a series connection between two or more cells: it allows to improve the performances of the solar device up to reach values of open circuit voltage enough high to power an external device. In fact, a three cells series connected module has been fabricated, leading to an output open circuit voltage of 2.14 V; this relatively high voltage is certainly an important result for practical applications, since they usually require units of Volts to be driven. Moreover, interesting results have been produced also for what concerns the bifacial-tandem configuration. It turns out that, with a parallel connection between two quasi-identical modules, the output photo-current corresponds more or less to the sum of the two single modules and so does the efficiency.

Beside this, also new materials have been employed, such to boost the ability in indoor conditions of a solar cell. Especially, a copper-based electrolyte together with a dye coming from the co-sensitization of XY1 and L1 have been deeply investigated, in order to reproduce literature results [22]. Actually, the study

carried on during this thesis activity do no lead to the same outcome find out by Michaels et al., but it certainly leave space for interesting discussions.
On the other hand, an EDLC has been proposed for the storage part, investigating at its working mechanism and physical principle. Then, different areas have been studied in order to find out capacitance and coulombic efficiencies. Finally, the best supercapacitor has been selected for the integration with the solar module. To this purpose, an EDLC with dimension of the active area 2cmx1cm has been chosen, showing a capacitance of 96.85 mF/cm^2 and a coulombic efficiency of 99.59 %.
In conclusion, the integrated HS device was proposed and its performances analysed. We have fabricate a three electrodes device, where DSSM counter electrodes and one of the two electrodes of the SC share the same FTO current collector. Actually, the integration between these two devices (DSSC and SC) was already further investigated during the last 10 years, but in this thesis activity an innovation has been proposed. Instead having just an integrated HS device, we have realized a bifacial-tandem integrated HS device, which exploits the benefits of bifacial-tandem connection longer studied during this activity. From a theoretical point of view, we expect that overall performances in terms of storage capacitance and combined efficiencies are able to reach higher levels, because of the presence of a parallel connection between the two energy harvesting devices.
By performing different analysis and focusing in particular on the photo-charge discharge process, we are able to make a comparison for both configurations.

Table 5.1: Comparison between integrated HS device and bifacial-tandem integrated HS device, from OPECSE analysis

Maximum OPECSE [%]	Voltage [V]	Time [s]
1.39	1.58	20
2.06	1.13	12

In particular, in table 5.1, the first column reports the maximum value achieved for the OPECSE in both integrated HS device and bifacial-tandem integrated HS device; the second column shows the voltage at which this maximum value is reached, while the last one express the time required to reach the maximum value for overall photon-to-electron conversion and storage efficiency.
We observe that the highest value of the combined efficiency (OPECSE) is 1.39 V, quite in agreement with literature (1.7 % from [33]). But let us consider this value retrieved for the bifacial-tandem device: an efficiency over 2 % is reached. Therefore, we can conclude that the integrated HS device proposed in this thesis allows to overcome the limits of efficiency that we have encounter in a standard integrated HS device.

The studies carried on so far make certainly the way to many other investigations and discussions. For instance, as mentioned during the course of this text, bifacial-tandem DSSM could be optimized by creating a device in which a unique counter electrode conductive on both sides is shared between both modules. To this aim, future works have been already planned in such a way to improve the design of the bifacial-tandem energy harvesting module. In fact, at first we could think to use a glue transparent to visible in such a way to have a stable and unique device, instead of two different ones simply put in contact [fig. 5.1].

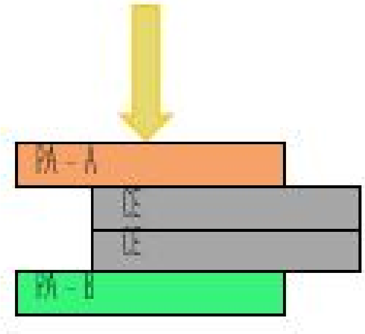

Figure 5.1: Design of the bifacial/-tandem dye sensitized solar module proposed in this thesis activity

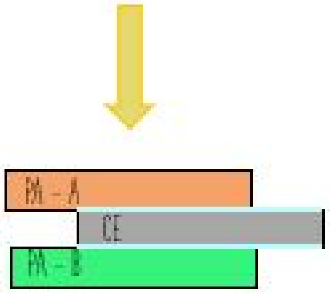

Figure 5.2: Design of the optimized bifacial/tandem dye sensitized solar module

Moreover, techniques for sputtering a conductive layer on the non-conductive side of the glass substrate have been already investigated [fig. 5.2]. ITO can be sputtered on that side in such a way to reach a configuration in which a unique counter electrode is shared between two photoanodes. This allows to reduce losses, since the incoming radiation should cross less interfaces in order to reach the bottom module.

Moreover, the fabrication process used to create the devices in our laboratory could be refined in order to have the possibility to create solar modules which are perfectly identical, in such a way to avoid losses and to decrease resistances. The experiments carried on so far have several parts that require high precision. Using hands instead of some technological machine implies lots of errors and poor precision. For instance, let us think at the way in which we create the active part sensitive to the incoming radiation. A tape is used as a mask and the desired shape is simply cut from it. This means that, actually, the masks used on the same dye-sensitized solar module or in different ones, could be not equal because of mistakes that can be performed from a human being, which is absolutely not so precise as a machine. Therefore, a first solution can be to used a screen printing

technique, where a more technological tool is used in order to establish where and how the active parts of harvesting devices are located.
On the other hand, considering the bifacial-tandem energy harvesting and storage device, improvements can be proposed. For instance, we can think to fabricate a device in which not only the harvesting part presents a bifacial-tandem configuration, but even the storage part does [fig. 5.3].

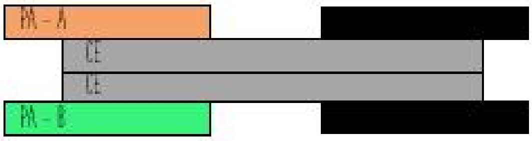

Figure 5.3: Schematic design of a bifacial-tandem integrated DSSM and SC

This means that together with two dye-sensitized solar modules in parallel, we will also have two capacitors in parallel. When two capacitance are put in parallel, they sum up while the resistances decrease. Therefore, this idea could lead to an enhancement of the storage ability of a supercapacitor and therefore to better overall performances of the device.

Bibliography

[1] B. Dorsemaine, J.P. Gaulier, J.P. Wary, and Nizar Kheir. «Internet of Things: a definition taxonomy». In: (2015) (cit. on p. 1).

[2] «https://www.nrel.gov/pv/cell-efficiency.html». In: (2021) (cit. on pp. 2, 3).

[3] Wikipedia. «https://en.wikipedia.org/wiki/Multi-junction$_{s}olar_{c}ellMulti - junction_{c}ells$». In: () (cit. on p. 4).

[4] Internet. «https://www.pveducation.org/pvcdrom/tandem-cells». In: () (cit. on p. 5).

[5] J. Wu, Y. Li, Q. Tang, G. Yue, J. Lin, M. Huang, and L. Meng. «Bifacial dye-sensitized solar cells: Astrategy to enhance overall efficiencybased on transparent polyanilineelectrode». In: (Feb. 2014) (cit. on p. 6).

[6] H. Michaels, M. Rinderle, R. Freitag, I. Benesperi, T. Edvinsson, R. Socher, A. Gagliardi, and M. Freitag. «Dye-sensitized solar cells under ambient light powering machine learning: towards autonomous smart sensors for the internet of things». In: (Feb. 2020) (cit. on p. 7).

[7] G Gautham Prasad, Nidheesh Shetty, Simran Thakur, Rakshitha, and K B Bommegowda. «Supercapacitor technology and its applications: a review». In: (2019) (cit. on p. 8).

[8] A. Hagfeldt, G. Boschloo, L. Sun, L. Kloo, and H. Pettersson. «Dye-sensitized solar cells». In: (2010) (cit. on p. 9).

[9] «GCell. Advantages of DSSC. [Internet]. GCell». In: (2020) (cit. on p. 10).

[10] M. L. Parisi, S. Maranghi, and R. Basosi. «The evolution of the dye sensitized solar cells from Grätzel prototype to up-scaled solar applications: A life cycle assessment approach». In: 39 (2014), pp. 124–138 (cit. on p. 12).

[11] «Gamry Instruments. DSSC: Dye Sensitized Solar Cells. [Internet]. Gamry Instruments.» In: (2020) (cit. on p. 13).

[12] Anees Ur Rehman, Farooq Aslam, and Haseeb Ahmad Khan. «Analyze the Absorption Properties and I-V Characterization of Dye Sensitized Solar Cell Using Ruthenium Dye». In: (Dec. 2014) (cit. on p. 15).

[13] T. McEvoy A.and Markvart and L Castaner. «Solar Cells. Materials, Manufacture and Operation. Elsevier, 2013, Second Edition». In: () (cit. on p. 16).

[14] A. Sacco. «Electrochemical impedance spectroscopy: Fundamentals and application in dye-sensitized solar cells». In: 79 (Jan. 2017), pp. 814–829 (cit. on pp. 17, 18).

[15] Solaronix. «Dye Solar cells For Real –The assembly guide for making your own solar cells». In: () (cit. on p. 19).

[16] Internet. «https://www.solaronix.com/documents/solaronix$_{m}$*aterials.pdf*». In: () (cit. on p. 20).

[17] K. Jena A and P. Bhargava. «Effect of amount of dye in the TiO2 photoanode on electron transport, recombination, Jsc and Voc of dye-sensitized solar cells». In: (Dec. 2012) (cit. on p. 23).

[18] A. U. Rehman, F. Aslam, and H. A. Kha. «Analyze the Absorption Properties and I-V Characterization of Dye Sensitized Solar Cell Using Ruthenium Dye». In: 161 (2014) (cit. on pp. 24, 25).

[19] L. Wang, X. Fang, and Z. Zhang. «Design methods for large scale dye-sensitized solar modules and the progress of stability research». In: (June 2010) (cit. on p. 25).

[20] D. Devadiga, M. Selvakumar, P. Shetty, and M. S. Santosh. «Dye-Sensitized Solar Cell for Indoor Applications: A Mini-Review». In: (2021) (cit. on p. 37).

[21] S. Hattori, Y. Wada, S. Yanagida, and S. Fukuzumi. «Blue Copper Model Complexes with Distorted Tetragonal Geometry Acting as Effective Electron-Transfer Mediators in Dye-Sensitized Solar Cells». In: (June 2005) (cit. on pp. 37, 38).

[22] H. Michaels, M. Rinderle, R. Freitag, I. Benesperi, T. Edvinsson, R. Socher, A. Gagliardi, and M. Freitag. «Dye-sensitized solar cells under ambient light powering machine learning: towards autonomous smart sensors for the internet of things». In: (2020) (cit. on pp. 38–41, 43, 44, 84).

[23] K.S. Srivishnu, S. Prasanthkumar, and L. Giribabu. «Cu(ii / i) redox couples: potential alternatives to traditional electrolytes for dye-sensitized solar cells». In: 2 (2021), pp. 1229–1247 (cit. on p. 42).

[24] N. Fadzilah, M. Sharif, S. Shafie, M.Z.A.Ab. Kadird, W.Z. Wan Hasan, M. Norhaffis Mustafa, and B. Samailac. «The effect of titanium (IV) chloride surface treatment to enhance charge transport and performance of dye-sensitized solar cell». In: 15 (Dec. 2019) (cit. on p. 42).

[25] L. Kavan, Y. Saygili, M. Freitag, S. Zakeeruddin, A. Hagfeldt, and M. Grätzel. «Electrochemical Properties of Cu(II/I)-Based Redox Mediators for Dye-Sensitized Solar Cells». In: 22 (Dec. 2017), pp. 194–202 (cit. on pp. 42, 43).

[26] A. Sacco, D. Pugliese, A. Lamberti, M. Castellino, A. Chiodoni, A. Virga, and S. Bianco. «A long-term analysis of Pt counter electrodes for Dye-sensitized Solar Cells exploiting a microfluidic housing system». In: 161 (2015), pp. 74–83 (cit. on p. 46).

[27] «https://www.andrew.cmu.edu/course/39-801/theory/theory.htm.» In: () (cit. on p. 51).

[28] M. S. Halper and J. C. Ellenbogen. «Supercapacitors: a brief overview». In: (Mar. 2006) (cit. on pp. 52, 55).

[29] A. M. Saleem, V. Desmaris, and P. Enoksson. «Performance Enhancement of Carbon Nanomaterials for Supercapacitors». In: (Mar. 2006) (cit. on p. 54).

[30] S. O. Okwundu, C. O. Ugwoke, and A. C. Okaro. «Recent trends in non-faradaic supercapacitor electrode materials». In: (July 2019) (cit. on p. 55).

[31] Y. Zhong, X. Xia, W. Mai, J. Tu, and Hong Jin Fan. «Integration of Energy Harvesting and Electrochemical Storage Devices». In: (2017) (cit. on p. 69).

[32] G. T. Kim, G. B. Appetecchi, M. Carewska, M. Joost, A. Balducci, M. Winter, and S.Passerini. «UV cross-linked, lithium-conducting ternary polymer electrolytes containing ionic liquids». In: (Sept. 2010) (cit. on p. 79).

[33] A. Scalia, A. Varzi, A. Lamberti, T. Jacob, and S. Passerini. «Portable High Voltage Integrated Harvesting-Storage Device Employing Dye-Sensitized Solar Module and All-Solid-State Electrochemical Double Layer Capacitor». In: (Sept. 2018) (cit. on p. 85).